NASA CONTRACTOR REPORT

NASA CR-200

NASA CR-200

PHOTOMETRIC MEASUREMENTS OF SURFACE CHARACTERISTICS OF ECHO I SATELLITE

by Richard H. Emmons, Harvey E. Henjum, C. L. Rogers, and Darrell C. Romick

Prepared under Contract No. NAS 1-3114 *by*
GOODYEAR AEROSPACE CORPORATION
Akron, Ohio
for

NATIONAL AERONAUTICS AND SPACE ADMINISTRATION • WASHINGTON, D. C. • APRIL 1965

NASA CR-200

PHOTOMETRIC MEASUREMENTS OF SURFACE CHARACTERISTICS OF ECHO I SATELLITE

By Richard H. Emmons, Harvey E. Henjum,
C. L. Rogers, and Darrell C. Romick

Prepared under Contract No. NAS 1-3114 by
GOODYEAR AEROSPACE CORPORATION
Akron, Ohio

for

NATIONAL AERONAUTICS AND SPACE ADMINISTRATION

For sale by the Office of Technical Services, Department of Commerce,
Washington, D.C. 20230 -- Price $3.00

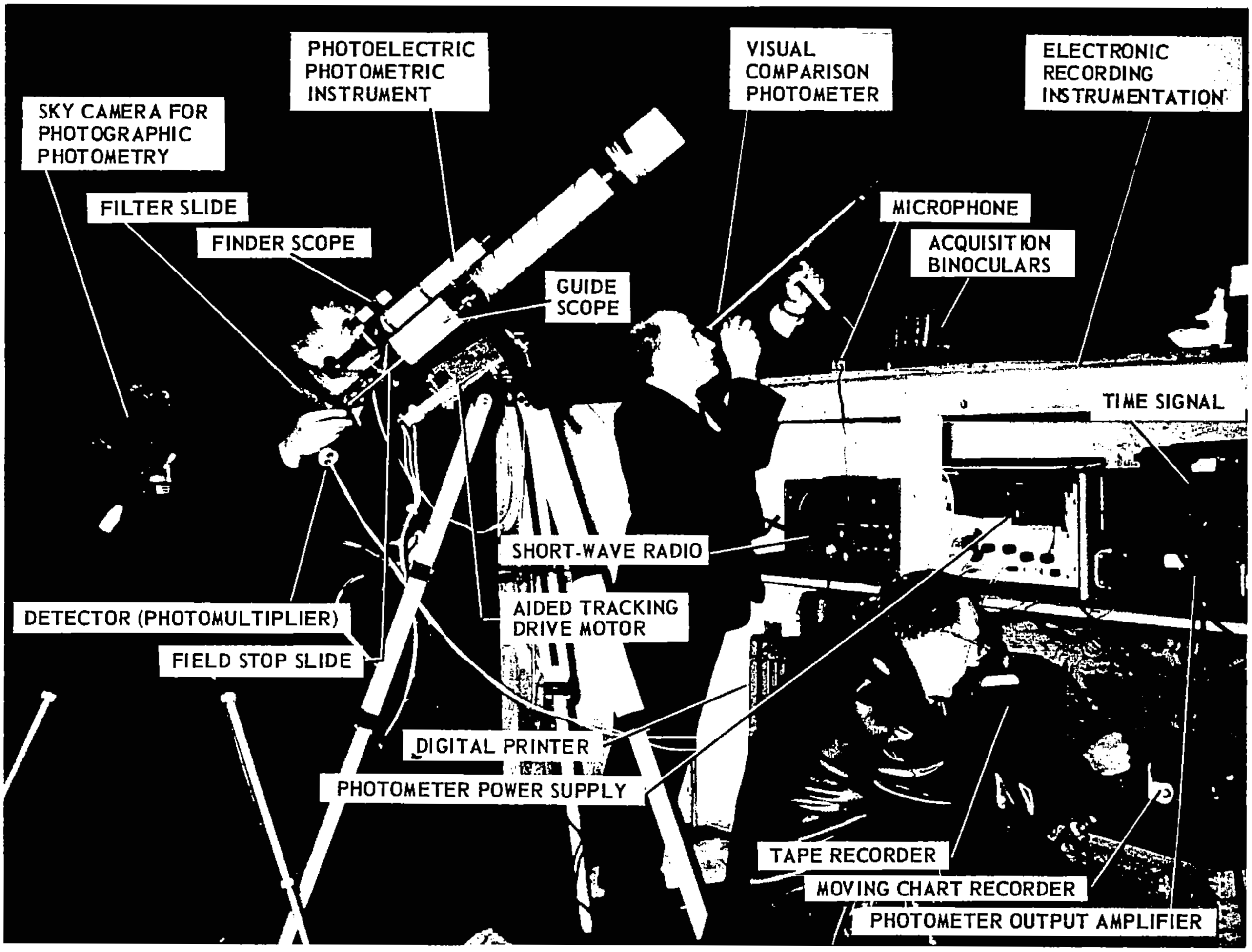

The Goodyear Aerospace Satellite Photometric Observatory Facility atop the Instrumentation Building at the Point Site of the Wingfoot Lake Radar Test Range

FOREWORD

This final report details a two-month task to measure and analyze the photometric characteristics of Echo I. This program was authorized under Amendment 5 of Contract NAS 1-3114.

Mr. William J. O'Sullivan, Assistant-to-the-Chief, Applied Materials and Physics Division, NASA Langley Research Center, provided technical direction for this task.

The principal Goodyear Aerospace Corporation participants are listed in alphabetical order. Richard H. Emmons, Harvey E. Henjum, C. L. "Bud" Rogers, and Darrell C. Romick.

ABSTRACT - SUMMARY

The results and techniques of a program that exploited the realistic test specimen represented by the nearly four-year-old Echo I Satellite by measuring its present surface characteristics are described. For this purpose, the classical astronomical techniques of photometric measurement were employed by developing and utilizing equipment and procedures for the measurement of satellite-reflected light. The data obtained thereby was analyzed to derive and evaluate the desired characteristics. Changes in specularity, reflectance degradation, over-all size, and present shape of the Echo I satellite are derived by this means.

In view of the time limitations involved and to assure validity of the results, it was decided to employ visual, photographic, and photoelectric photometry simultaneously. This permitted correlation of results and determination of the strong points, weaknesses, and most appropriate use of each method. During the program period, all needed equipment was assembled and procedures developed to give satisfactory operation. Data was taken during every satisfactory pass with suitable weather. The Russel phase-angle-luminance relationship was used to derive specularity-to-diffuse ratio. Results obtained from analysis of this data indicated that nearly all of the initial specularity remained, that reflectance had decreased very little (less than 10 percent) over the four-year period in the earth-orbital space environment, and that the mean diameter had reduced very little although significant local surface variations were measured. Good correlation existed in results obtained from the three different methods. A wealth of other information beyond the scope, objectives, and time limitations of this program was also found to exist in the data (especially the photoelectric traces) obtained. The basic feasibility of the method employed was proven, and the far wider inherent potential capability of these techniques was demonstrated by this initial venture into this technology. Therefore, the program was extremely successful.

TABLE OF CONTENTS

LIST OF ILLUSTRATIONS

LIST OF TABLES

SECTION I. INTRODUCTION

The 100-foot diameter Echo I satellite was successfully deployed in orbit after launch from Cape Canaveral on August 12, 1960 (Reference 1). It was fabricated from 1/2-mil Mylar film with an outside coating of vapor-deposited aluminum nominally 2000 Å thick. Therefore, the aluminized Mylar surface of Echo I has been exposed to micrometeoroids and other factors of the near-earth environment for nearly four years. This represents a significant opportunity for any characteristic changes to such surfaces to be developed if they were going to occur within a reasonable time period. Any changes in its initially specular and highly reflecting surface would be of immediate value in the technology of materials for space applications and to the scientific study of the environmental factors.

Reference 2 describes a first attempt to determine Echo I's surface characteristics by photometric means. The present report describes the effort under Amendment 5 of Contract NAS 1-3114 to verify and refine the results of the earlier study. The raw photometric data from the earlier study has since been subjected to the digital computer reduction, processing and analysis programs applied to the subsequent data in this study. This recomputation utilized improvements in both the orbit and theory over that used in the original manual processing of the data. The original data was reprocessed in this study for comparison purposes and has been separately identified herein as obtained from observed pass "number 0".

Table I presents the dates on which photometric observations were made of Echo I. These observations were taken utilizing clear atmospheric observing conditions during periods ("windows") of visibility with wide phase range (see Figure 1). Alternately in the morning and evening visibility periods, Echo I's trajectory becomes more nearly aligned to the sun, permitting observations over a wide range

Table I. Photometrically Observed Echo I Passes

Pass No.	U T Date 1964	Site	Visibility Period	Remarks
0	1 March	SAO Station No. 8544	Evening	Visual only
1	25 April		Morning	Visual only
2	25 April		Morning	Visual only
3	26 April		Morning	Visual only
4	2 May		Morning	Visual only
5	2 May		Morning	Visual only
6	3 May		Morning	Visual only
7	3 May		Morning	Visual only
8	4 May		Morning	Visual only
9	4 May		Morning	Visual only
10 (1)(2)	28 May	GASPO (WFL)	Evening	Visual plus photoelectric
11 (2)	28 May		Evening	Visual plus photoelectric
12 (2)(3)	28 May		Evening	Photoelectric only
13	30 May		Evening	Visual plus photoelectric
14 (2)(4)	30 May		Evening	Visual plus photoelectric
15 (2)(4)	2 June		Evening	Visual plus photoelectric
16 (2)(4)	2 June		Evening	Visual plus photoelectric
17	5 June		Evening	Visual plus photoelectric

(1) Visual data not processed.

(2) Photoelectric data not processed.

(3) Visual data not taken.

(4) Visual data processed but rejected; large calibration σ (battery problem).

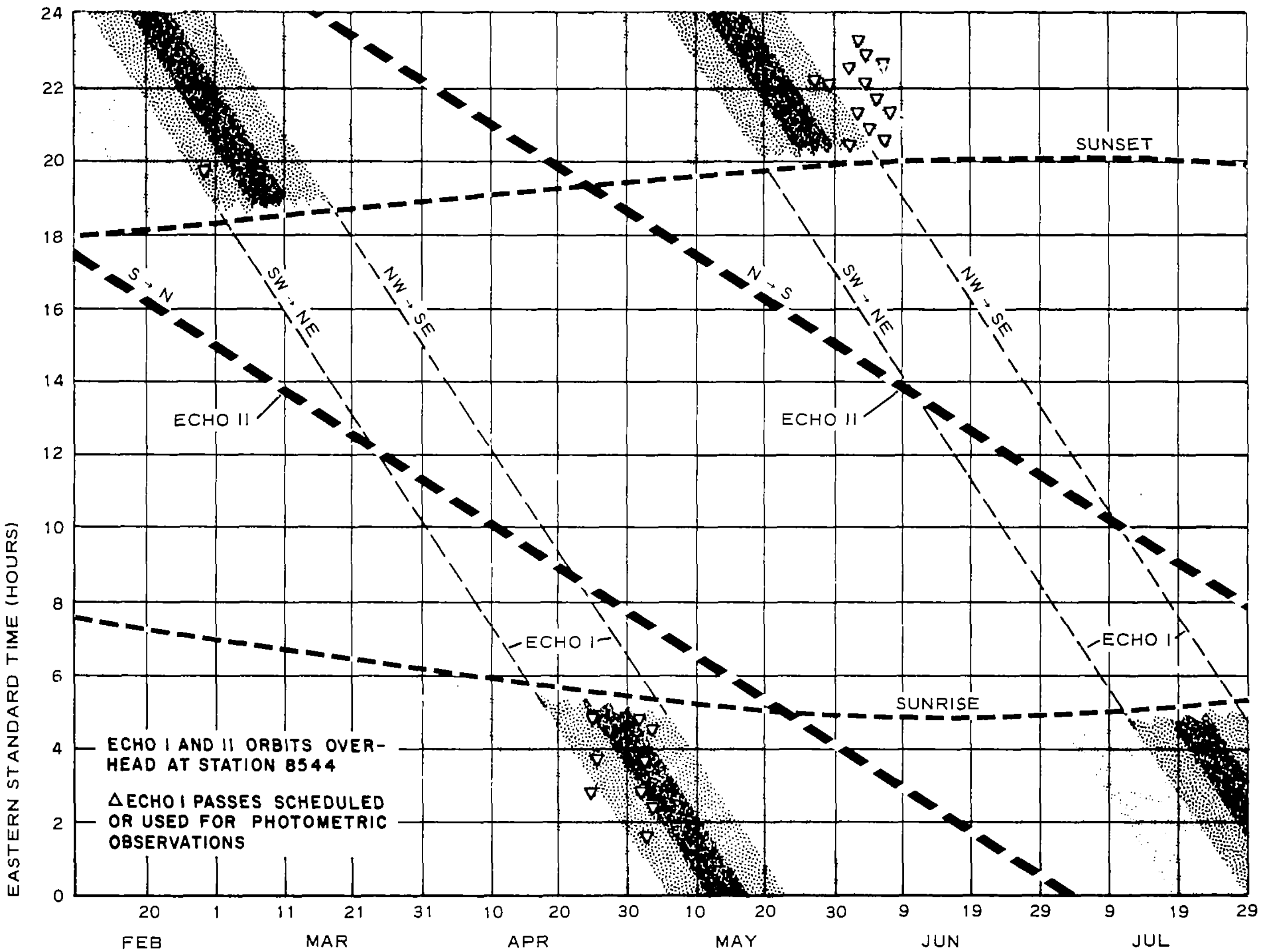

Figure 1. Satellite Observing "Window" Availability Diagram for Period of This Program

of phase angles. The 0 pass was observed in the evening, passes 1 through 9 were observed in the morning, and passes 10 through 17 were observed in the evening.

The approach used to best assure fulfillment of the objectives of this program was to employ all three of the classically developed methods of photometric observation utilized by conventional astronomy. By using all three for this new application to satellite photometry, developing suitable instrumentation and techniques for each, it was possible to explore and partially evaluate the relative suitability and validity of each method, as well as to cross-correlate the results of each appropriately to yield maximum validity and accuracy to the final results. Accordingly, the visual photometric observations were always backed up by simultaneous photographic observation, and as soon as the photoelectric equipment could be placed in satisfactory operation, all three methods of photometric observations were employed simultaneously.

Two sites were employed for the observations: Smithsonian Astrophysical Observatory (SAO) satellite tracking station No. 8544 and the Goodyear Aerospace Satellite Photometric Observatory (GASPO) site (see frontispiece) at Goodyear's Wingfoot Lake (WFL) facility. Figure 2 shows the latter site and location. The coordinates of these sites are given in Table II.

The symbols and terms used in this report are given in Table III.

Table II. Observing Site Coordinates

Site	W Longitude	N Latitude	Altitude (MSL)
SAO Station No. 8544	81° 24' 42.0"	40° 52' 44.9"	350 meters
GASPO (WFL)	81° 22' 05"	41° 00' 54"	360 meters

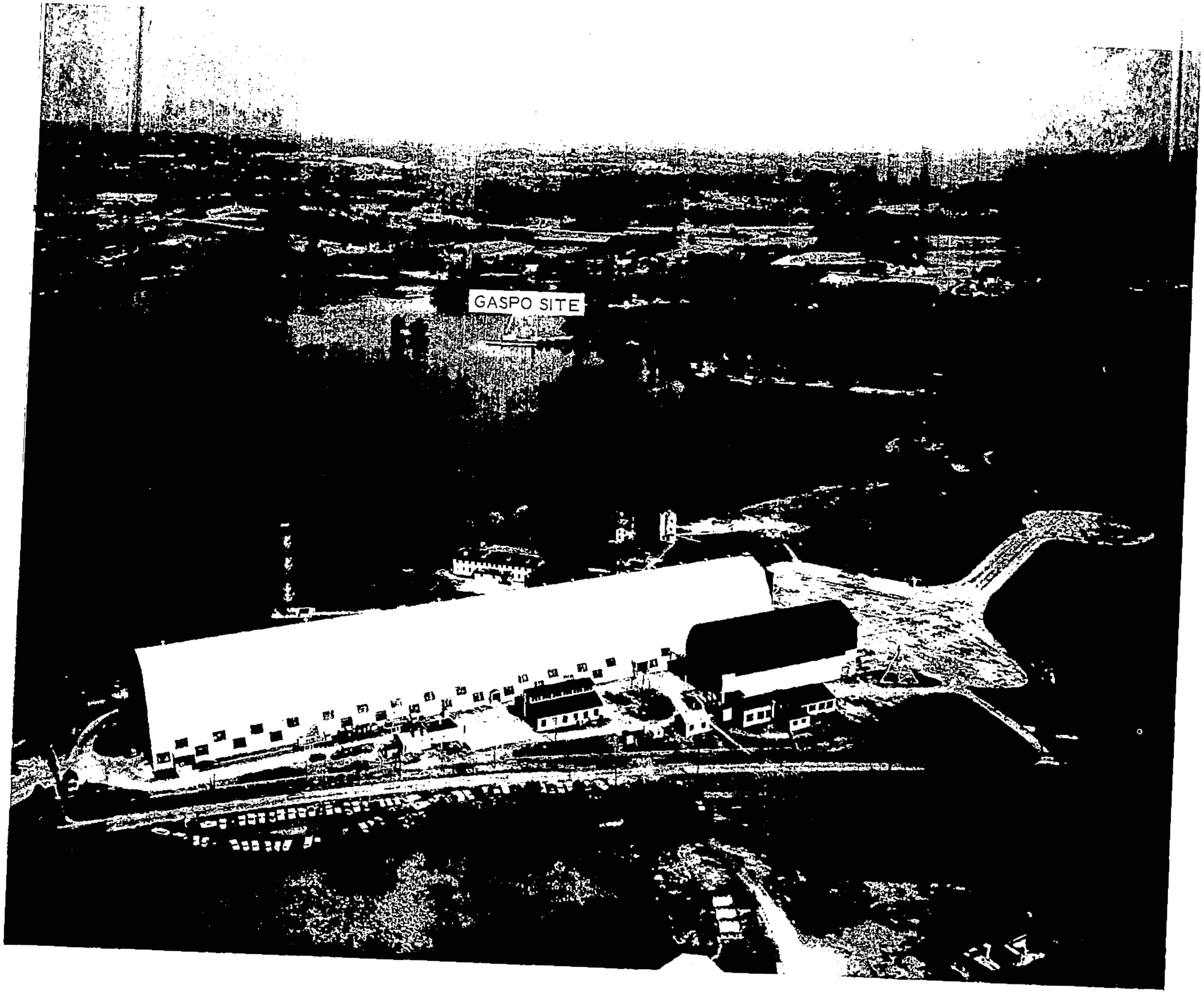

Figure 2. GASPO WFL Site

Table III. Symbols and Terms

Symbol/Term	Definition
a	Constant used in calibration equation
b	Coefficient used in calibration equation
k	Atmospheric extinction coefficient (Δm)
m	Extra-atmospheric stellar magnitude
m_0	Satellite m, adjusted for earth albedo and normalized to 1000 st mi range
m_{sp}	Indicated specular magnitude; m_0 less diffuse contribution
pe	Probable error
r	Correlation coefficient
t	Student's t test, time
z	Angular zenith distance (degrees)
A	Weighting coefficient for optically specular reflection, area
B	Weighting coefficient for optically diffuse reflection
D	Distance (miles)
Dec	Declination (degrees)
E	Illuminance
E_0	Illuminance of a zero magnitude star
E_s	Illuminance of the sun at earth's orbit
F	Function, luminous flux
IR	Instrument reading
R	Satellite radius (feet)
RA	Right ascension (hour angle)
R_c	Satellite radius of (compound) curvature (feet)
UT	Universal time (day, hour, minutes, seconds)
X	Effective number of zenith atmospheres

Table III. Symbols and Terms (Continued)

Symbol/Term	Definition
γ	Coefficient of reflectivity
σ	Standard deviation
ψ	Satellite phase angle (0 deg when "full") (degrees)
ω	Angular velocity, relative
Illuminance	The luminous flux incident on a surface per unit area; $E = dF/dA$.
Luminosity	The luminous flux density emitted by a remote body
Magnitude (stellar)	The arbitrary brightness measure assigned to a celestial body in accordnace with the relationship $m = -2.5 \log (E/E_0)$ where E_0 is an arbitary luminosity represented by zero magnitude
Reflectivity or Reflectance	The ratio of the intensity of the light reflected by a surface to that of the incident light falling upon it
Specularity	Degree of specular reflectivity. Usually expressed in percentage of total reflectivity, meaning that portion of light reflected in accordance with the laws of (specular) reflection; i. e., the angle of reflection (with the plane of the reflecting surface) is equal to the angle of incidence.
Diffusivity	Degree of diffuse reflectivity. Usually expressed in percentage of total reflectivity, meaning that portion of light reflected in accordance with Lambert's cosine law of diffuse reflection; i. e., the radiant intensity of a plane surface area falls off as the cosine of the angle between the normal to the surface and the direction of the observer.
Regression (equations)	The statistical relationships used to find the mean or most probable values among samples involving two or more related variables, and thereby defining the "lines of regression" (a terminology generated by its original application to hereditary genetic distributions).

SECTION II. THEORY

A. GENERAL

The present investigation, like that of Reference 2, is a new application of the established science of photometric astronomy. From careful measurements of the intensity of sunlight reflected from an artificial satellite, various inferences can be drawn concerning the present condition of its surface. In the photometric study of the Echo I satellite, the first consideration was to determine, if possible, the extent to which its initially specularly reflecting surface had become roughened or diffuse-reflecting during its almost four-year exposure in the near-earth space environment. For this analysis, the following assumptions were made:

(1) The diffuse component in the sunlight reflected from Echo I will obey the Russell phase function (Equation 1), or will not deviate from it to an extent that would significantly affect the conclusions.

(2) The earthshine component of the light reflected from Echo I is equal to that predicted on the basis of a spherical specular satellite.

B. MICROTEXTURE

The diffuse reflection determination is referred to as microtexture analysis. The distinctly different optical behavior of specular and diffuse spheres is apparent by simply comparing a shiny Christmas tree ornament with a snowball.

A specular sphere has a convex mirror surface that provides a small image reflection of the sun, equal in "brightness"* regardless of the viewing angle.

*Illuminance, E; stellar magnitude = $-2.5 \log_{10} (E/E_0)$.

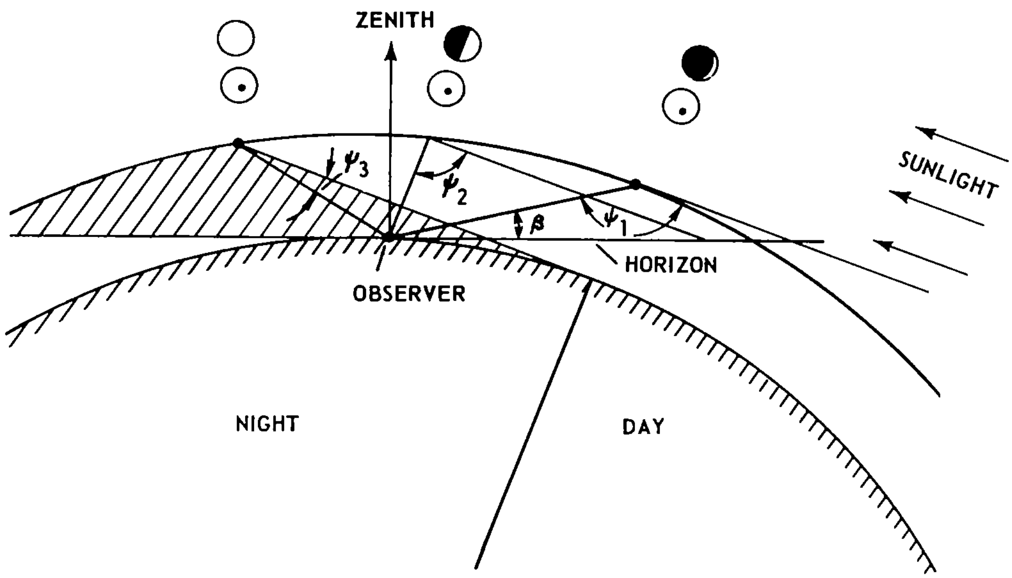

Figure 3. Satellite Phase Geometry

For a 50-foot radius specular sphere, the sun's image is only 2.8 inches in diameter. A diffuse sphere in sunlight exhibits "phases," like the moon. The integrated light from the diffuse sphere is a function of the "phase angle", ψ, defined as the angle at the sphere between the light source and the observer (zero when phase is "full") (see Figure 3).

H. N. Russell (Reference 3) provides the relation between the observed brightness and the phase angle for a perfectly diffuse sphere that obeys Lambert's Cosine Law of Reflection*:

*This law states that the reflection from a small area is proportional to the product of the cosine of the angle between the incident light and the normal to the surface and the cosine of the angle between the normal and the direction to the observer.

$$\frac{E}{E_0} = F(\psi) = \frac{1}{\pi}[\sin\psi + (\pi - \psi)\cos\psi] . \quad (1)$$

R. Tousey (References 4 and 5) provides the equations by which the brightness of diffuse and specular satellites may be compared:

$$\text{Specular case:} \quad \frac{E_{sp}}{E_0} = \frac{1}{4}\frac{R^2}{D^2}\frac{E_s}{E_0} = 10^{-0.4m} \quad (2)$$

$$\text{Diffuse case:} \quad \frac{E_d}{E_0} = \frac{2}{3}\frac{R^2}{D^2} F(\psi)\frac{E_s}{E_0} = 10^{-0.4m} \quad (3)$$

where

- R = radius of the satellite,
- D = distance of the satellite, $(D \gg R)$,
- E_s = solar illuminance on the satellite,
- E_0 = illuminance value at zero stellar magnitude,
- m = stellar magnitude.

Equations 2 and 3 then provide the basis for photometrically discriminating between specular and diffuse spherical reflecting surfaces. From a series of brightness observations at various determinable and widely ranged phase angles of a spherical satellite, the relative contributions of simultaneous specular and diffuse reflections can be found. It follows by appropriate scaling that the regression equation permitting this determination is (as used in Reference 2)

$$\frac{E}{E_0} = 10^{-0.4m} = \frac{1}{4}A + \frac{2}{3}B F(\psi) \quad (4)$$

where

- A = weighting coefficient for optically specular reflection,
- B = weighting coefficient for optically diffuse reflection.

The indicated specularity is then $\frac{A}{A + B}$. (5)

Before Equation 4 may be applied, however, the reduced observed satellite magnitudes must all be further processed to

(1) Correct for atmospheric extinction.

(2) Normalize to a uniform satellite distance (herein, 1000 st mi).

(3) Correct for the contribution of earth albedo.

The first of these corrections depends upon the atmosphere's zenith filter factor, k (expressed in magnitudes), at the time of the observations and the effective number, X, of such atmospheres through which the light passes. X is a function of the object's zenith distance, z. This function is given, together with a discussion of the determination of k, in Section IV, "Calibration" paragraph.

Normalization of the photometric data to a uniform range is accomplished simply by applying the inverse square law of illumination to the illuminances, first having determined the satellite's slant range at each observation time (see Section IV, "Calibration" paragraph). The correction for the contribution of the earth's albedo ("earthshine") for a specular spherical satellite is a function of the satellite's orbital height and central angle from the sun (References 6 and 7). Figure 4, taken from Reference 6, presents the magnitude increments based on a 0.37 earth albedo and a specular spherical satellite.

Note that the indicated specularity resulting from Equations 4 and 5 is virtually independent of calibration index errors that might occur between observed passes of the satellite, permitting observations throughout various passes to be safely accumulated in the regression solution.

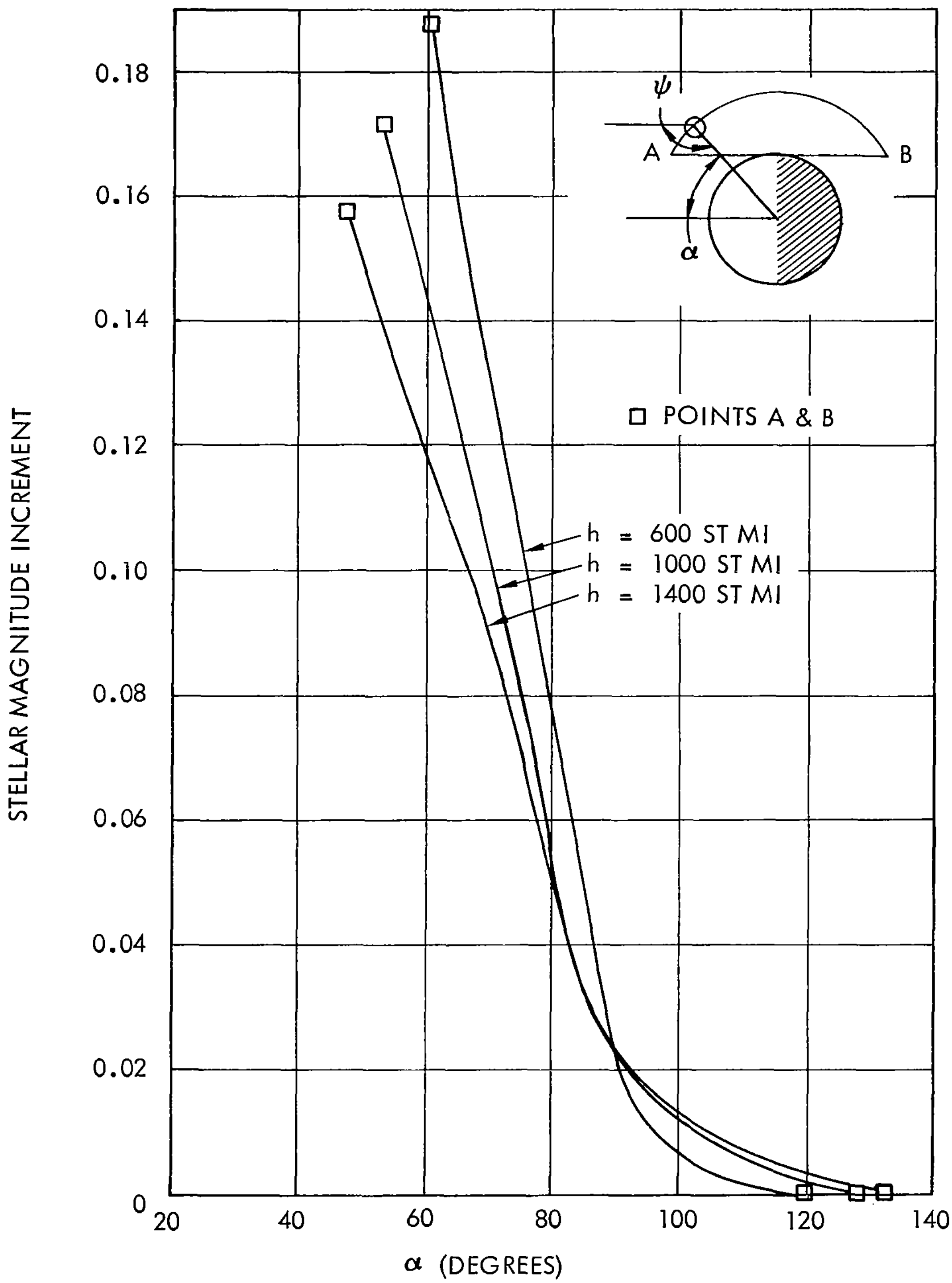

Figure 4. Stellar Magnitude Increment of Specular Sherical Satellite due to Earth Albedo

C. MACROTEXTURE

The second consideration in the photometric study of Echo I was to obtain mean and local effective radii of (compound) curvature, R_c, of the satellite and to note extreme values. This is referred to as macrotexture measurement and analysis.

Having determined the diffuse-reflecting weighting coefficient, B, in the preceding microtexture analysis, it is now possible to remove from the normalized magnitudes the contribution of diffuse reflection in each, $-2.5 \log 2/3 \, B \, F(\psi)$, to obtain purely specular magnitudes, m_{sp}. If a reasonable value for the specular reflectance*, γ , is then chosen, the radii of curvature can next be determined from the relation (Reference 8),

$$R_{c(ft)} = \text{antilog} \, (+ 1.6776 - 0.5 \log \gamma - 0.2 \, m_{sp}). \quad (6)$$

Since laboratory tests of mildly "aged" aluminized Mylar yield γ values between 0.80 and 0.85, a γ of 0.83 was chosen for the R_c determinations herein.

A third consideration in the Echo I photometric studies was the reflectivity, γ , itself.

Since the observed illuminances depend on both γ and R_c (see Equation 6), one may be obtained only if the other is known or assumed. From the previously discussed macrotexture analysis methods, a mean radius of curvature can be obtained, assuming $\gamma = 0.83$. Also obtained were local radii of curvature, the range and variability of which may be examined in light of the original design and available material for gross implications for a possible new mean radius of curvature. For example, if <u>all</u> the somewhat randomly "observed" radii of curvature were first found to be much greater than the designed 50 feet, the previously assumed value of γ could well be challenged as being too small.

---

*Not to be confused with specularity.

Macrotexture variations do exist, and neglecting material stretch, these would tend to reduce the true mean R_c below 50 feet. On the other hand, there is danger that satellite stabilization might act to bias the observed areas from the true mean R_c. The logical solution (within the scope of this program) for the problem of reflectivity was to provide a parametric solution of γ against R_c. Very fortunately for the analyst, the results of this study tend to relax the ambiguity in the reflectivity, providing moderately high reflectivities even at what was regarded as a reasonable upper limit mean radius of curvature.

Although the specularity determination was virtually independent of between-pass index errors, this is not true of the macrotexture and reflectivity analyses. Considerable care was taken during the calibrations to minimize this problem, and some processed data was later rejected on the basis of apparent index error. It is believed that any remaining between-pass index errors of the data used do not significantly affect the conclusions of this investigation.

SECTION III. INSTRUMENTATION

A. VISUAL-COMPARISON PHOTOMETER

The visual-comparison photometer used in this investigation is detailed in Figure 5. It is shown in actual use in the frontispiece photograph. The rotating polarizing filter is controlled by the Microdial, adjusting the brightness of the comparison point of light to that of the reference star (during calibration) or to the satellite. Upon achieving a match in brightness, the observer says "mark", which is picked up by a nearby microphone together with Bureau of Standards time signals from the short-wave radio set to WWV, and tape recorded. The digitized filter angle provided by the Microdial is then read into the tape recorder with the aid of a red-filtered flashlight. Between observations, the filter angle is returned to zero, requiring a completely independent "hunt" for the next brightness match. An experienced operator can make and read-out observations as frequently as five times per minute, although it is not felt desirable to try to maintain such a high data rate. Experience during actual calibration against reference stars in various parts of the sky yields standard deviations as low as 0. 14 magnitude, depending sensitively on the photometric uniformity of the atmosphere. Where precalibration and post-calibration observations throughout the sky have been combined, the resulting dispersions increase to about 1/4 magnitude, one case reaching 0. 326. Since the satellite data was taken in between the calibration periods, it is reasonable to assume that the satellite data is not subject to these extreme dispersions.

B. PHOTOGRAPHIC BACK-UP

A tripod-mounted, 124 mm, f 4. 5 Kodak 616 roll film camera having a field of

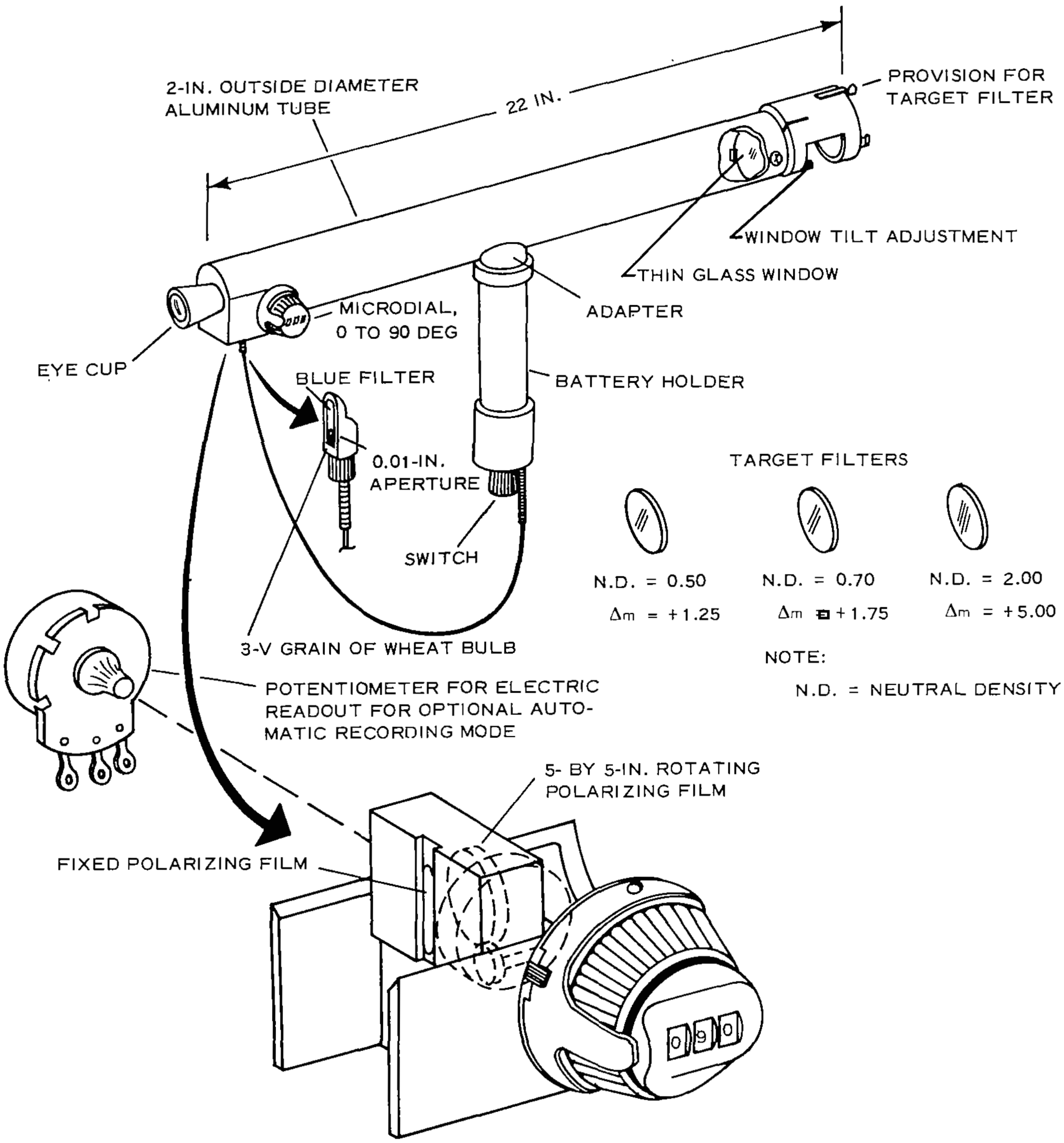

Figure 5. Visual Comparison Photometer for Bright Satellites

view of approximately 30 x 45 degrees was used with Verichrome pan film (ASA rating 125) to record the Echo I trail against star trails during one- and two-minute sequential exposures during the pass. Figure 6 is a two-minute exposure showing Echo I passing through the Big Dipper's handle. Over 50 such photographs were taken during the program. Resolution achieved was well below 100-second arc, judging from the clean trails obtained of both components of the "double" star Epsilon Lyrae (separation 207 seconds), as can be clearly seen with a magnifying glass.

Times of "shutter open" and "shutter closed" were tape recorded along with the superimposed CHU or WWV radio time signals, thus providing adequate tracking information to check and, if necessary, slightly amend the mean anomaly equation of the acquisition orbital elements furnished by SAO for subsequent phase angle, elevation, and slant range determinations.

The Echo I trail photographs also provided a back-up record of gross brightness variations. These photographs have also been examined to confirm the absence of local thin cloud effects upon the photometric data. Several instances of bright star "sideswipe" were recorded on the photographs, and photoelectric data at these times were not used in the analyses.

Figure 7 is an enlarged section of a photograph (frame 7, roll 6) taken during pass 7 from $08^h\ 47^m\ 20^s$ to $08^h\ 49^m\ 21^s$ UT on 3 May 1964 from site 8544, while the satellite was moving from RA $23^h\ 37^m$ Dec + 15. 9° to RA $23^h\ 55^m$ Dec + 08. 5°. Careful visual comparison under magnification of the densities of the Echo I trail in the vicinity of its intersection with star 82 Pegasi and the trails of the stars in Table IV indicated that the Echo I trail at this point had the density equivalent of a solar-type (G2) star of magnitude 5. 2.

The possible effect of the different displacements of Echo I and these stars from the optical axis was investigated and found to range from 0 to only 0. 02 magnitude on the basis of the fourth power of the cosine, and was therefore neglected.

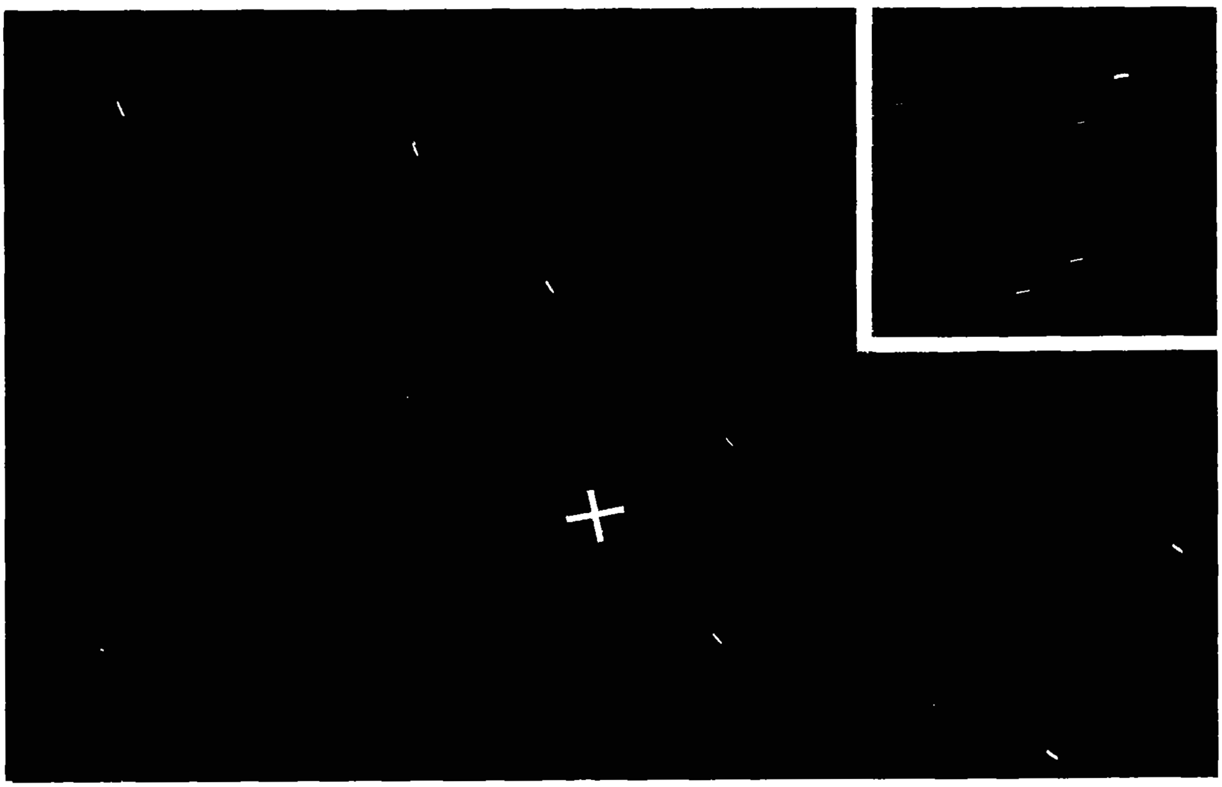

Figure 6. Echo I Passing through Big Dipper's Handle (Inset Shows ϵ Lyrae Double from Roll 1, Frame 3 - See Text)

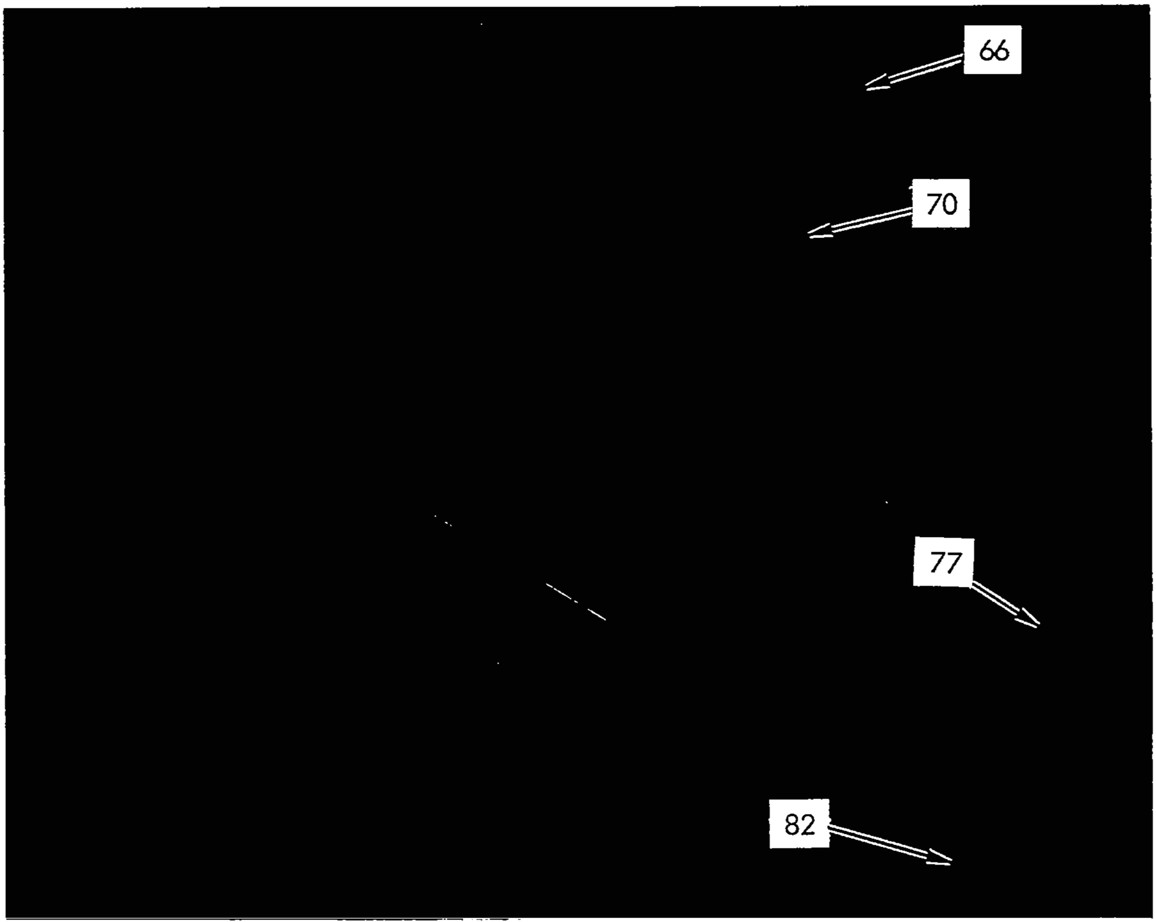

Figure 7. Echo I Passing near Star 82 Pegasi

Table IV. Reference Star Data (for Figure 7)

STAR	SPECTRAL CLASS	VISUAL MAGNITUDE
66 Pegasi	K4	5.28
70 Pegasi	G9	4.67
77 Pegasi	M2	5.39
82 Pegasi	A2	5.39

The resulting 5.2 magnitude is to be compared with +2.32 obtained from the visual photometer at this time, the difference being attributable to the angular velocity ratio between Echo I and the reference stars. The average mean angular velocity ratio can be readily approximated by measuring the relative lengths of the satellite and star trails when the satellite trail limits are both available on the photograph. In this instance, the angular velocity ratio had to be computed, and the result was 17:1.

The theory of trailed images (Reference 11) leads to the conclusion that the difference in photographic magnitudes resulting from different angular velocities is simply

$$m = -2.5 \log_{10} (\omega_1/\omega_2).$$

On this basis, the magnitude increment that would be expected from an angular velocity ratio of 17 is -3.07, which appears too large. Agreement between the photometric and photographic magnitudes can, however, be attained by instead applying a $(\omega_1/\omega_2)^{0.93}$ correction, resulting in a $\Delta m = -2.86$. This empirically determined $(\omega_1/\omega_2)^{0.93}$ correction was found to give excellent agreement with visual photometric measurements in three additional applications, leading to its use in the final pass (17) to establish an additional point at high-phase angle. This "photographic point" is shown plotted with the visual photometric data for pass 17 but was not included in the machine analysis for specularity.

Figure 8(A) shows a microdensitometer trace down the Echo I trail of Figure 7. Note that the interference from the several wires in the photograph are easily seen. Similar data is shown in the trace of Figure 8(B). Although the use of the microdensitometer for this investigation was briefly explored, results were uncertain, and it did not appear feasible to pursue this approach within the scope of the present program, although the possible potential value and information content of this method were indicated.

C. PHOTOELECTRIC INSTRUMENTATION

1. Telescope

The basic sensor element of the photoelectric instrumentation consisted of a telescope of optimum aperture for first or second magnitude work, mounting, a photomultiplier along with suitable guide and acquisition telescopes. The telescope used was the "Galactic" model distributed by the Lafayette Radio Corporation. Of basic interest is the 910 mm focal length with a 76.2 mm clear aperture for the primary telescope and the 500 mm focal length with a 42 mm clear aperture for the "finder" telescope. The telescope and associated parts are described in Figure 9. The 76.2 mm telescope was used for photoelectric light gathering, and the 42 mm telescope was used for tracking. Visual angles of from 0.3 to 2 degrees were attainable on the tracking telescope from the eyepieces furnished with the telescope and without recourse to the 25 x magnifier. The 20 mm Huygen eyepiece with a visual angle of 2 degrees was found to be suitable for use in this application. An additional telescope with a visual angle of approximately 7 degrees was incorporated as an acquisition aid and substantially increased the continuity of coverage.

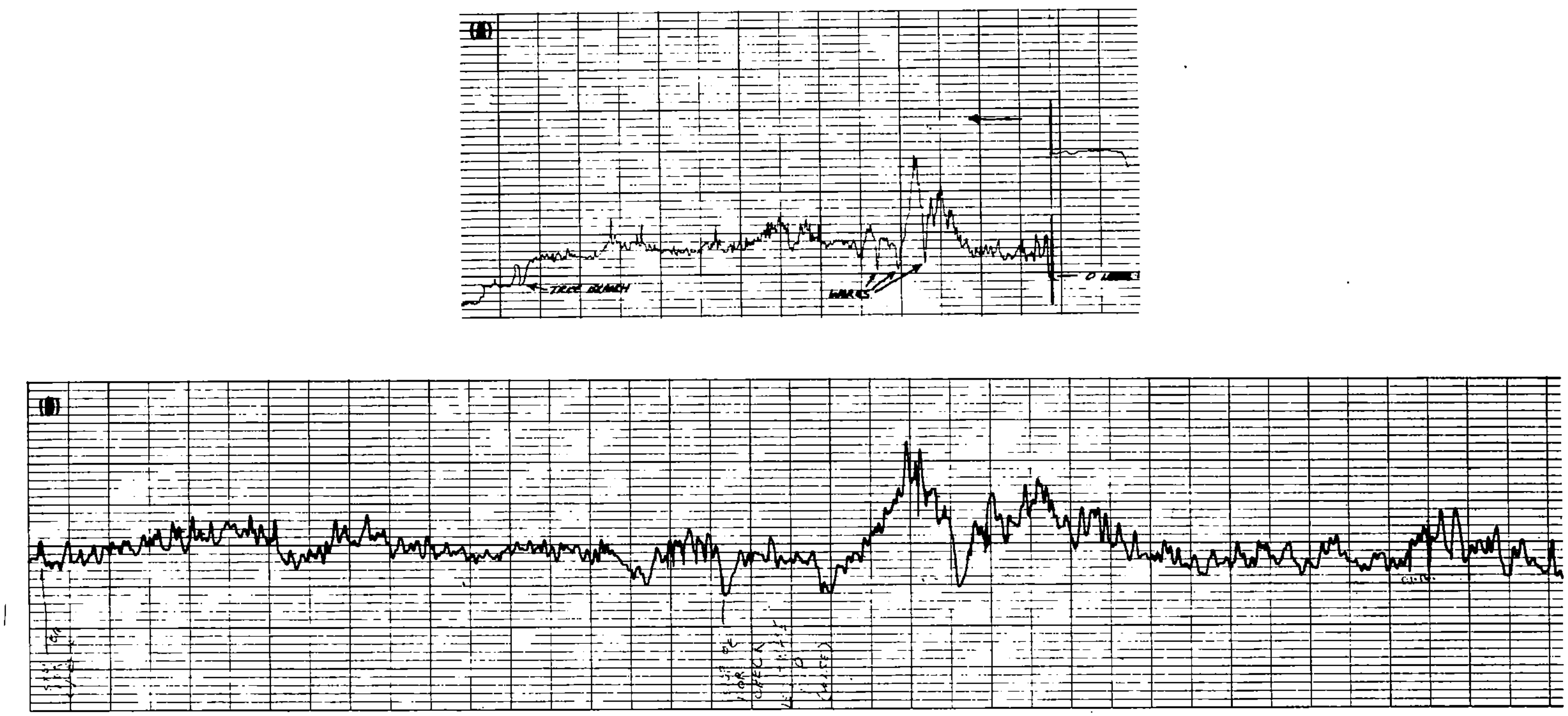

Figure 8. Microdensitometer Trace of Echo I Trail in Figure 7

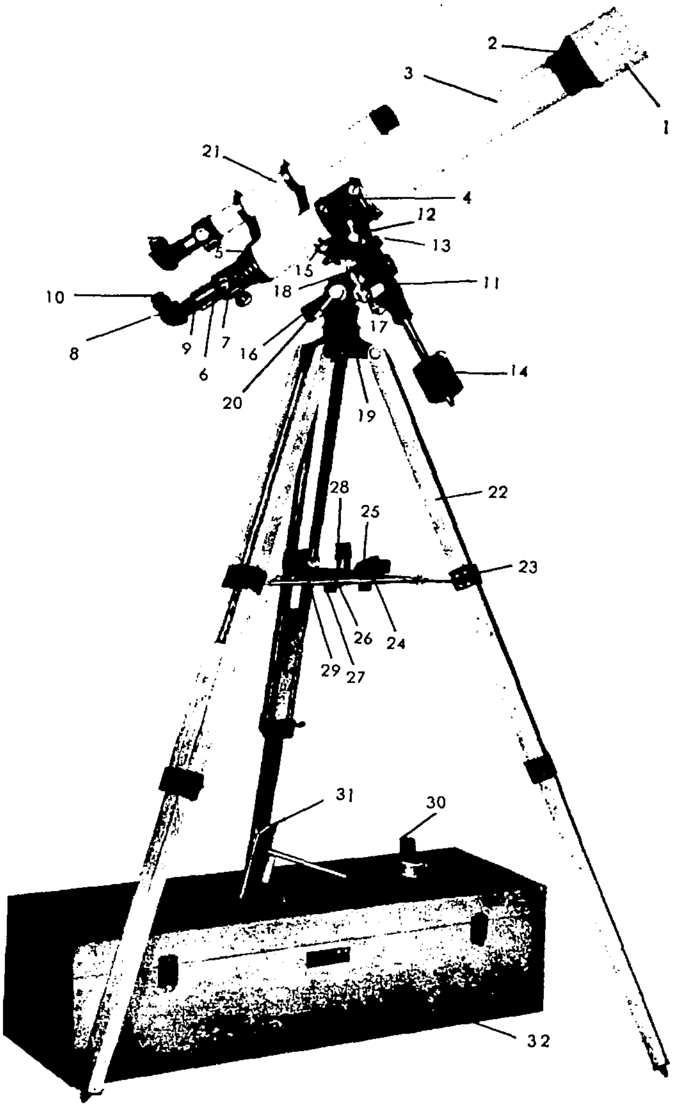

1. Dew cap (Lens hood)
2. Objective cell
3. Telescope tube
4. Telescope tube trunnion sleeve with clamp screw
5. Eye end
6. Eyepiece drawtube with rack and pinion motion
7. Micro focusing knob for eyepiece
8. Star diagonal
9. Eyepiece adapter
10. Eyepiece
11. Declination axis
12. Clamp lever for fixing the telescope to the Declination axis
13. Declination circle
14. Adjustable counter-poise of the telescope with respect to the polar axis (Balance weight)
15. Slow motion in declination
16. Polar axis
17. Slow motion in Right Ascension
18. Hour circle
19. Tripod head with adjustment in Latitude
20. Clamp lever fixing the inclination of the polar axis
21. Finder telescope
22. Two section wooden field tripod
23. Tripod reinforcing band
24. Accessories tray
25. Sun diagonal
26. Eyepiece (HM 6mm)
27. 〃 (HM 12.5mm)
28. 〃 (H 20mm)
29. Sun-glass
30. Erecting prism
31. Sun projecting screen
32. Wooden carrying case

Figure 9. Components of the Telescope

The problem of dew deposit was minimized by slightly elevating the temperature of the telescope assembly via the use of household "gutter cable" as a distributed heating element.

2. Photoelectric Adaptation

The primary telescope was adapted for photoelectric use through addition of a photoelectric detector assembly at the eyepiece draw tube. The detector assembly used was Shoeffel Instrument Co model D-500 and incorporated an RCA 1P21 photomultiplier tube. Leads were lengthened to 8 feet to allow full telescope traverse, and the original mounting tube was replaced with an aluminum adapter mount specifically designed to accommodate insertion of a field (Fabry) lens and a filter selector bar. A further adaptor tube was designed to mate the mounting tube to the eyepiece draw tube and accommodate field selection via graded aperture holes in the focal plane of the telescope. An adapter to permit interchange of the photoelectric system with the 42 mm telescope was also fabricated for possible alternate usage. Design was based on the following criteria:

(1) Focal plane - field selector congruence at near mid-range of rack and pinion adjustment for both telescopes.

(2) Nominal adjustment of field lens at center of adjustment range.

(3) Accessibility for testing and adjustment as required.

The fabricated pieces are shown in Figure 10.

3. Optical Design

Design of the optics of the photoelectric system was directed toward meeting the requirements of (1) obtaining a suitable size image of the objective lens on the photomultiplier cathode, (2) providing for suitable field of view via aperture selection, and (3) obtaining suitable color match with visual observations.

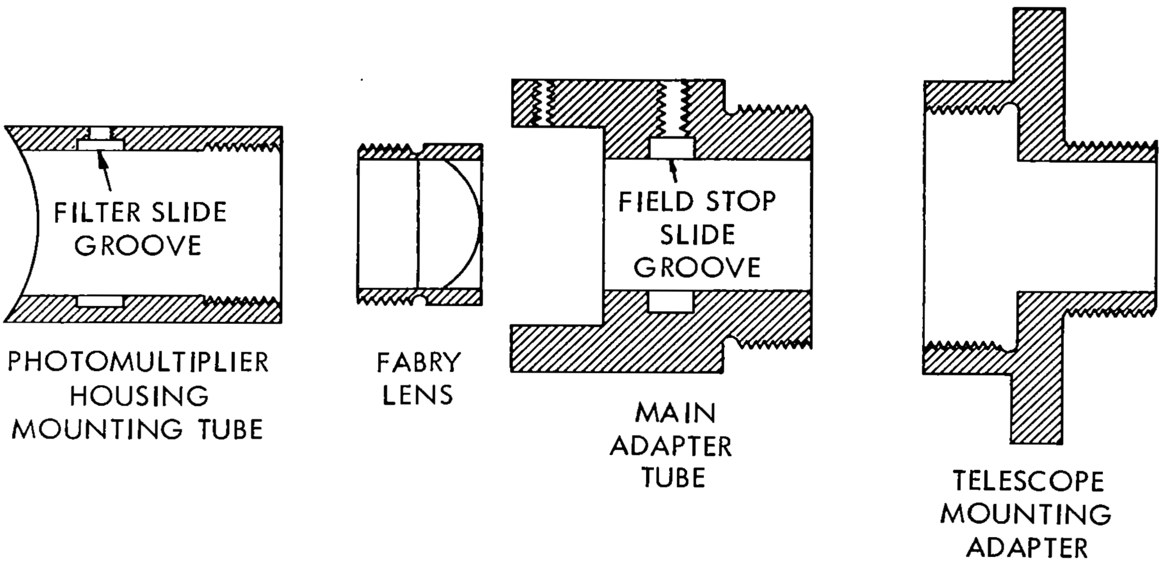

Figure 10. Adapter Assembly for Photoelectric Equipment

The size of the objective image on the photomultiplier cathode is initially considered with the Fabry lens assumed to be exactly on the focal plane (910 mm from the objective lens). The field (Fabry) lens chosen was a Jaegers 18 mm diameter lens with a focal length of 49 mm.

The effective focal length of the field lens for a real image of the objective is calculated as follows:

$$\frac{1}{f_e} = \frac{1}{f_f} - \frac{1}{f_o}$$

$$= \frac{1}{49} - \frac{1}{910}$$

$$= 0.0204082 - 0.0010989$$

$$= 0.193093.$$

$$f_e = 51.79 \text{ mm.}$$

The image size, I, is calculated by considering the central ray through the lens in the following manner:

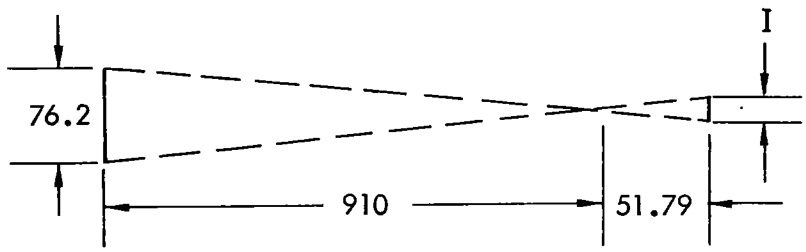

$$I = \frac{51.79}{910}(76.2)$$

$$= 4.34 \text{ mm}$$

$$= 0.171 \text{ inch.}$$

Since the field stop must be located in the focal plane, the Fabry lens is actually located at approximately 922 mm from the objective. The realized image is then calculated as

$$\frac{1}{f_e^1} = \frac{1}{49} - \frac{1}{922}$$

$$= 0.19323.$$

$$f_e^1 = 51.75.$$

$$I^1 = \frac{(51.75)(76.2)}{922}$$

$$= 4.27 \text{ mm}$$

$$= 0.168 \text{ in.,}$$

which is compatible with the projected region of best collection for the 1P21 photoelectric tube as shown:

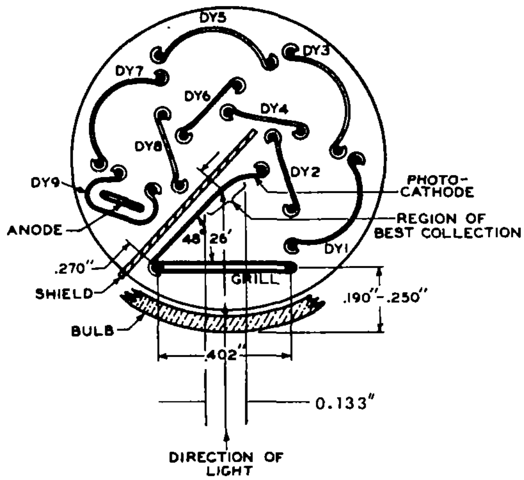

The field of view at the aperture stop is calculated using the central ray through the lens as follows:

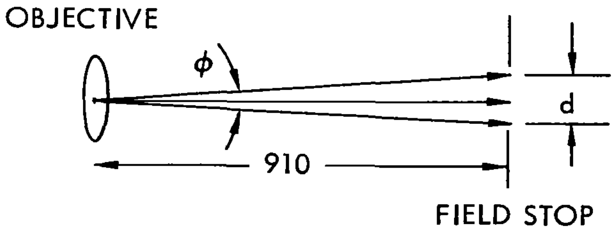

$$\tan \phi = \frac{d}{910}$$

The following tabulation indicates field stops and corresponding fields of view as incorporated in the slide mounted in the main adapter tube:

d (mm)	ϕ(degrees)	Relative Field Area
16	1.007	16
11.3	0.713	8
8	0.503	4
5.6	0.353	2
4	0.252	1

In use, sky background brightness made using the larger field stops undesirable. Twenty-two millilambert radioactive phosphorescent light sources were procured from Dial Service and Manufacturing Company of Cleveland and installed behind these slide stops, thus allowing a system gain check to be made as part of the regular operating procedure.

Since a comparison between visual and photoelectric measurements was required for this study, filter type GG14 obtained from Fish and Shurman was used for all photoelectric measurements (although the other filters for the U, B, V system were also mounted in the filter slide). This filter effectively limited the photoelectric response to that characterized by the visual spectrum.

4. Electronic Instrumentation and Recording Equipment

Instrumentation for the acquisition of data is shown in Figure 11. The M600 Photometer provided high voltage for the photomultiplier tube and initial stages of amplification. The Brush Amplifier model BL530 provided additional adjustable amplification and the Dual Channel Recorder, Brush model BL202, allowed a permanent record to be made.

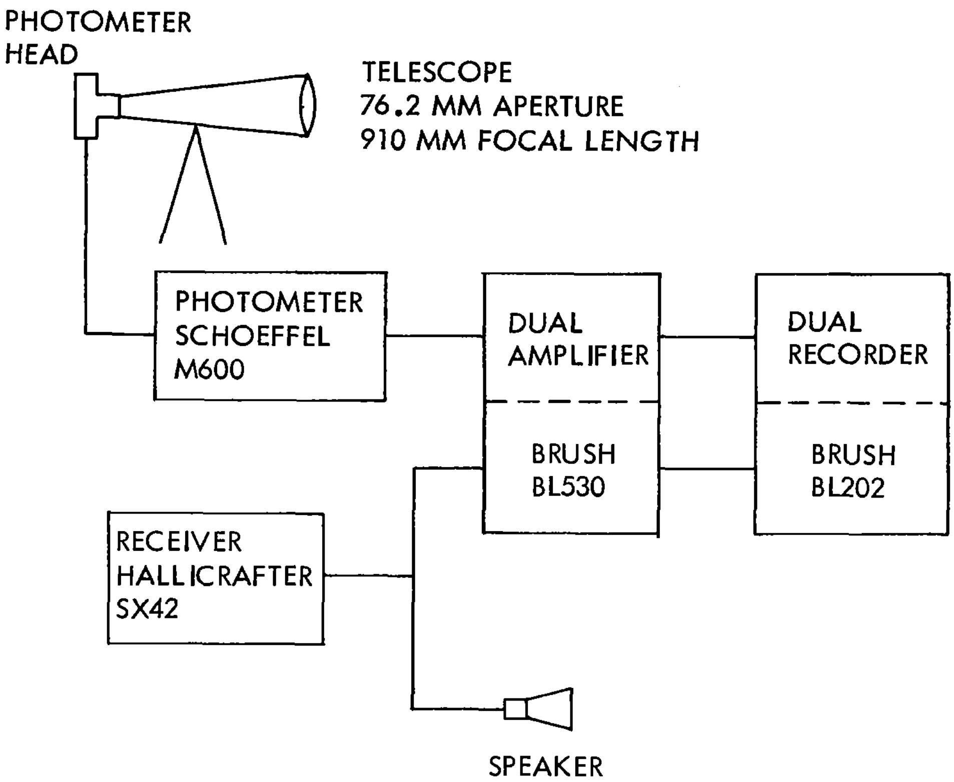

Figure 11. Photoelectric Instrumentation

WWV signals were received solidly on either the 10 mcs band or the 5 mcs band through use of the Hallicrafter model SX42 receiver. An envelope detector was required to be inserted between the receiver and the recorder amplifier to provide for proper pen response.

Other accessories that provided useful information during the test were the magnetic recorder, microphone, and variable speed motor control for "aided" tracking.

5. Acquisition and Tracking

Acquisition and tracking of the satellite during most of the runs were by manual means, although motor-driven aided tracking was also provided. Figure 12 shows the various freedoms available in the mount.

The plane best fitting the satellite position locus and the observer is estimated using the altitude and azimuth of the satellite at culmination. The telescope and its various freedoms are fixed in accordance with the figure. Tracking is then attained with right ascension variation and small amounts of corrective changes in declination as the pass is monitored.

The tripod mount did not allow this mode of operation for overhead passes in that mechanical restriction of the telescope was present when θ approached 90 degrees. A corrected mount was designed but not implemented during this program.

Control of the telescope position was attained by presetting the friction forces on the declination and right ascension restraints such that the telescope could be manually moved through the positions required for satellite monitoring throughout the pass.

In this mode, control with the 5. 6 mm stop was such that almost continuous monitor could be attained. The 4 mm stop would allow about 80 percent monitor and was used on NASA pass 13, since periodic background illumination level readings are necessary for data reduction.

Aided track with a drive on the right ascension freedom axis was used during initial phases of monitor and allowed an estimated 2:1 increase in control accuracy. This mode was not used in acquiring data for NASA passes 13 and 17 because of mount restrictions on high-altitude passes as mentioned above.

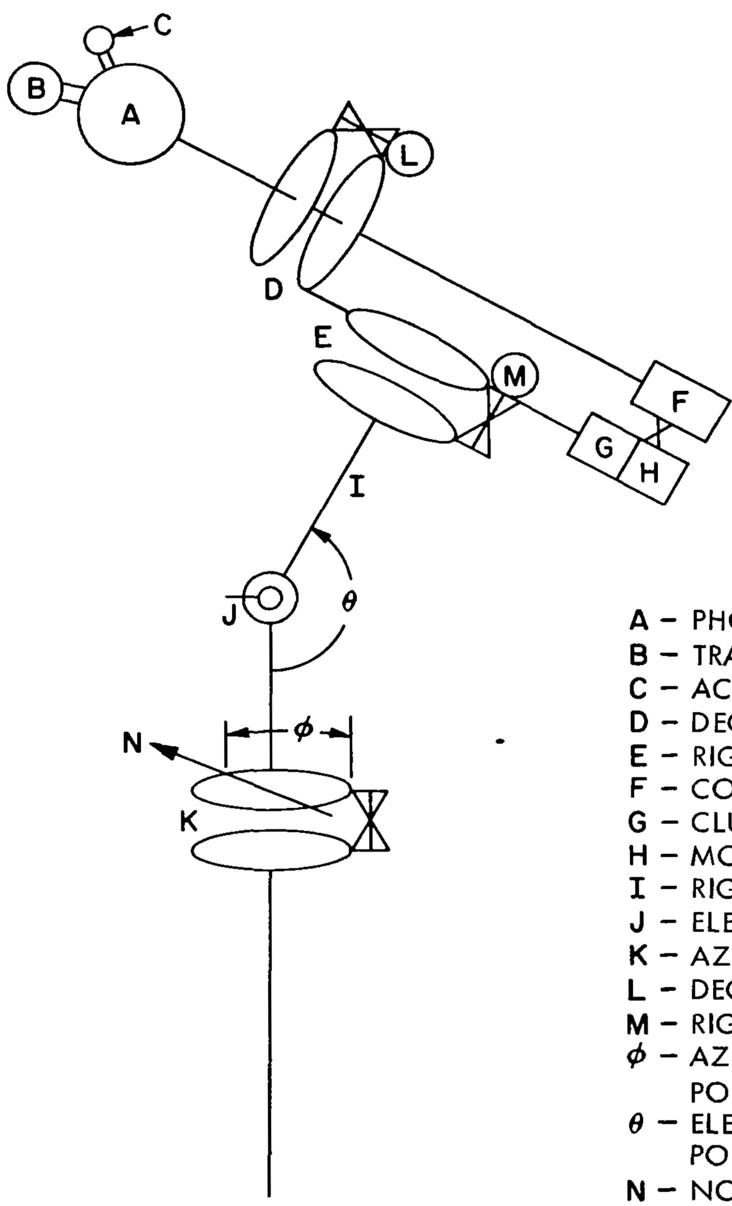

A – PHOTOELECTRIC TELESCOPE
B – TRACKING TELESCOPE
C – ACQUIRING TELESCOPE
D – DECLINATION FREEDOM
E – RIGHT ASCENSION FREEDOM
F – COUNTERWEIGHT
G – CLUTCH
H – MOTOR - GEARHEAD
I – RIGHT ASCENSION POLE
J – ELEVATION FREEDOM
K – AZIMUTH FREEDOM
L – DECLINATION MANUAL DRIVE
M – RIGHT ASCENSION MANUAL DRIVE
ϕ – AZIMUTH OF RIGHT ASCENSION POLE AT CULMINATION
θ – ELEVATION OF RIGHT ASCENSION POLE AT CULMINATION
N – NORTH

Figure 12. Telescope Mount Alignment Features

6. Calibration

Calibration of all data was made with respect to star magnitudes. Linearity of the amplifiers, gain drift, and zero drift were monitored and incorporated into calibration where required. The radioactive light source was used to illuminate the photomultiplier before and after pass 17 to confirm that over-all system gain had not changed. Readings of "zero level", amplifier calibration, voltage level, and adjacent sky background level were interspersed during data recording to provide adequate calibration data.

Several special checks are required to ensure that correct "Fabry" action is being utilized in the telescope optics. First,the field stop aperture must be located at the focal plane. This is checked by slipping off the photoelectric head and adjusting the rack and pinion for a clear star (or other light source) image on a piece of wax paper temporarily bonded to the aperture. The second special check is to pass a star through the field of view at a constant rate. Various adjustments of Fabry lens distance are made until maximum slope on the record at the field edge indicates correct positioning of the objective image on the photomultiplier cathode.

SECTION IV. DATA PROCESSING AND ANALYSIS

A. GENERAL

The reduction and analysis of the observational data obtained required first putting the data in a point tabulation form, i. e., reducing it to a series of data points for each pass in the form of values proportional to the light received at the observing sensor from the satellite or calibration star. Next, use of the calibration star readings and the associated geometry of the observations must be normalized to comparable extra-atmospheric magnitude values. Then the resulting data must be processed and analyzed to extract the desired satellite surface characteristics. The data flow, shown in Figure 13, is described in the following paragraphs.

B. DATA REDUCTION

The visual photometric observing process utilized gave data point readings proportional to the observed object directly from the recorded Microdial readings. However, where the observational data is in the form of raw signal traces or other output, as in the case of the photoelectric method, it must be reduced to such data point readings.

Data readings are made from the recorded signal trace with several points in mind:

(1) Desired readings must be in terms of the additional light in the field which is generated by the satellite (or star) only.

(2) Scintillation is present because of the small telescope used.

(3) Macrotexture variation is present because of variation in curvature of the satellite surface.

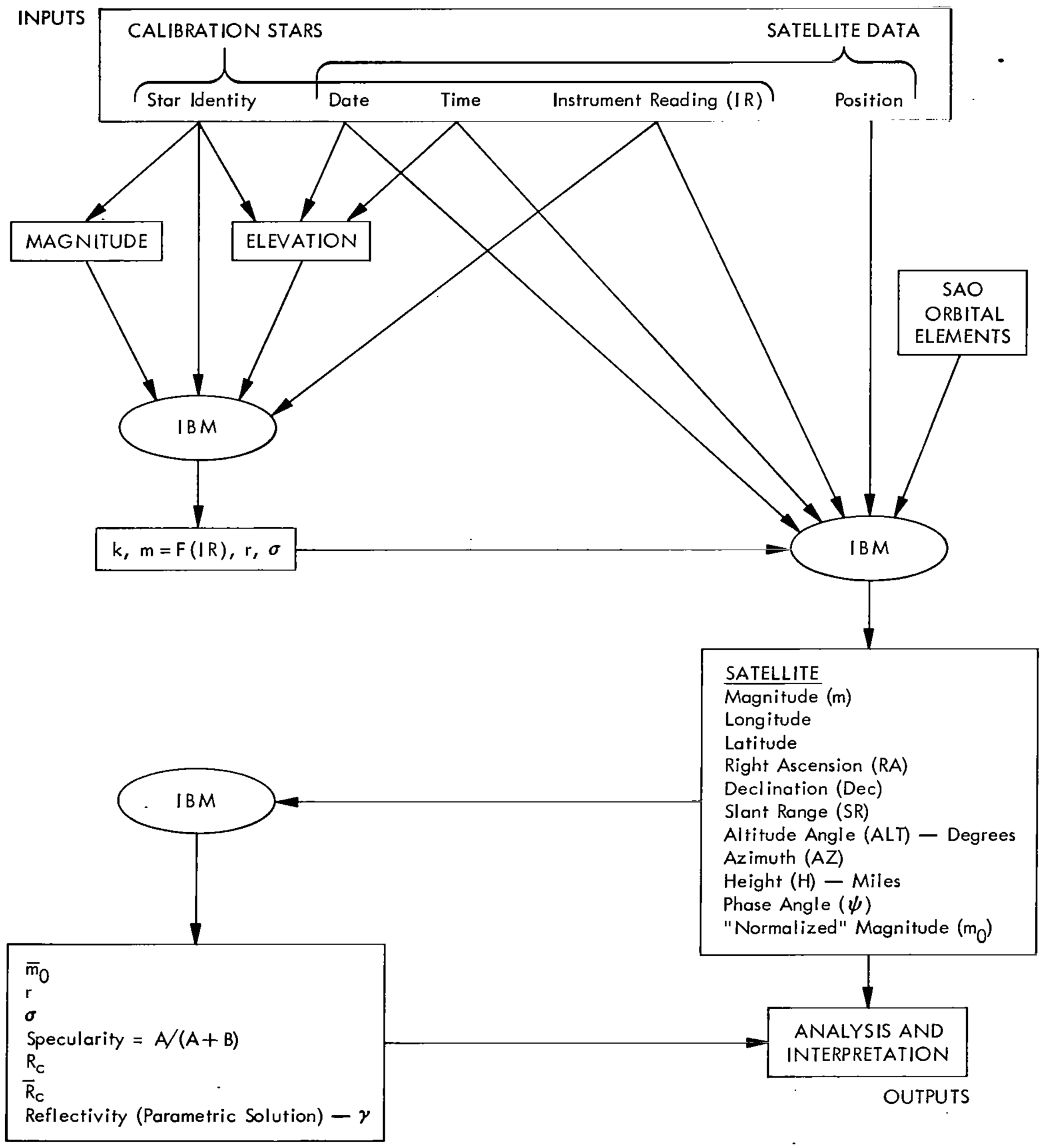

Figure 13. Data Flow Diagram

(4) The instruments are operated such that linear gain characteristics are attained.

(5) In some areas of the sky, thin cloud cover could be present although not visible to the observer. This may lead to throwing out of one or several of the calibration star data used in obtaining atmospheric transmission coefficients.

The type of data recorded by the equipment is shown in Figure 14, which shows typical star calibration data recorded on NASA pass 16 and satellite luminosity data recorded on pass 17, including its eclipse in the earth's shadow (bottom line). The WWV radio time signal trace is recorded above each data trace.

Noteworthy features of this typical data are the calibrating star identification notations (Regulus, γ Leonis), the gain setting notations (e.g., "11-6" - meaning the amplifier gain range settings of the photometer and d-c signal amplifier feeding the recorder, respectively), the sky background levels recorded (and noted) at appropriate intervals, and the calibration levels (labeled "cal" in the notation). Zero level settings are also recorded periodically (see Figure 15). Also note the pulse (or pip) recorded each second on the time signal trace, plus WWV identifying code, coded time indication, voice modulation (giving same information), and resumption of 440-cycle modulation tone following this, with the superimposed 1-second interval pulses.

It can be noted in this data (especially the center trace of Figure 14), as well as in the photographic photometry trace (Figure 8), that there are three distinct frequencies observable in the light output signal trace. One is a relatively high frequency of about 4 to 6 cycles per second, representing scintillation effects. Another is a medium frequency with a period of around 5 to 8 seconds, while a third lower frequency variation appears to have a period of from 15 to 20 seconds. There are also other variations, but these latter two must surely represent

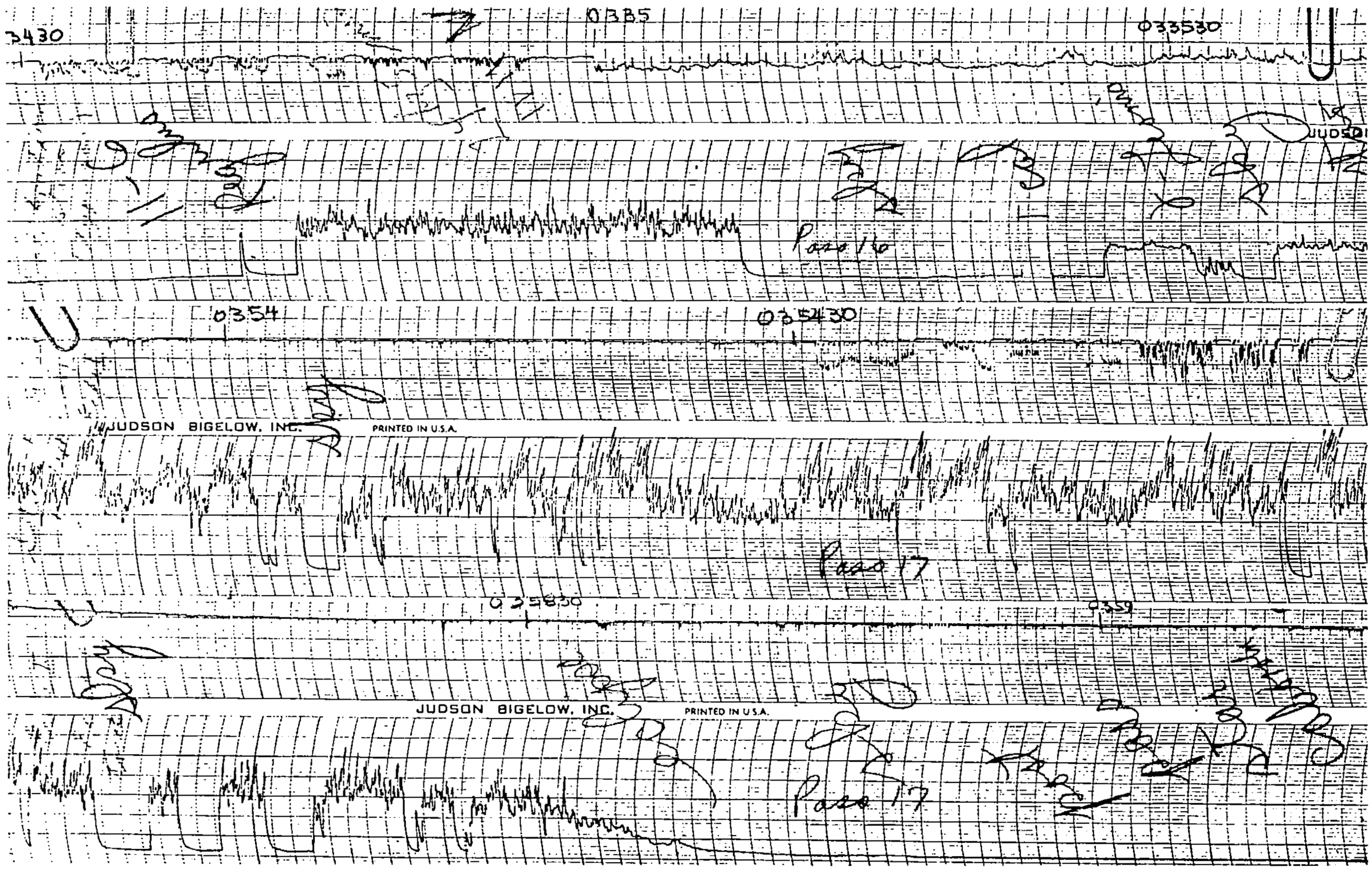

Figure 14. Typical Recorder Data

effects of the satellite surface geometry (macrotexture), position geometry, and attitude dynamics. Since the investigation and analysis of these aspects were beyond the scope of this program, the main consideration here was to utilize data reduction and analysis techniques that would eliminate their effect.

For illustration of the data read-out processes, several examples of typical data used in calibration and during satellite passes are shown in Figures 15 through 18. As can be seen in these figures, superimposed lines are drawn representing average signal levels (thus excluding the higher frequency and scintillation variations) at frequent intervals along the signal trace. The readings for seven typical data points (15 through 21) and two calibration star levels (representing two gain setting levels) are shown, along with time reference indications on the corresponding time signal traces.

These signal levels are then measured with reference to the "cal" level (see signal traces) from the sky background level base line and "zero" levels (also shown). These data readings (along with their gain settings) are then tabulated, and in succeeding columns manipulated in accordance with the calibration equation. This data forms the input to the computer programs, and the reduction process proceeds from this point identically the same as with each method.

It can be seen that several factors in the received light intensity (and resulting signal) contribute to the accuracy limits to which the data can be read. For example, the macrotexture contribution to confidence limits is quite evident. Factors that might be reduced and approaches are as follows:

(1) Scintillation: By use of a larger telescope.

(2) Amplifier gain and zero drift: By true differential signal handling or chopping in the focal plane.

(3) Tracking alignment: By error driven mount.

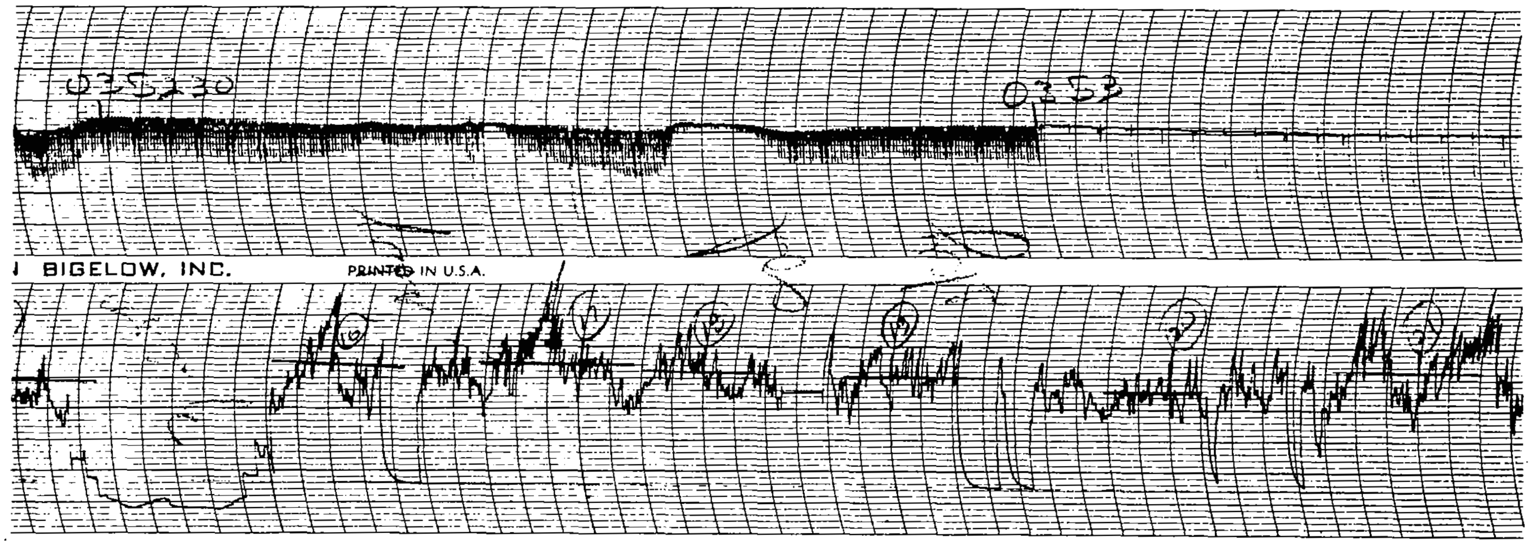

Figure 15. Satellite Data Illustrating Reduction Point Selection and Macrotexture

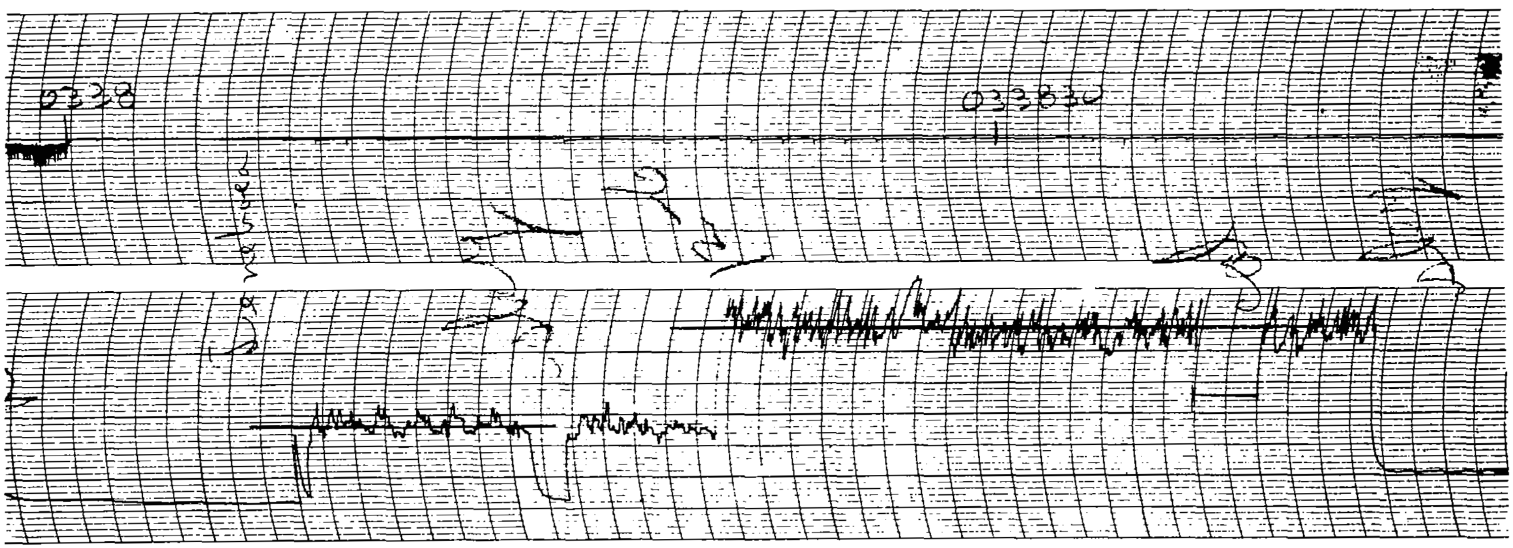

Figure 16. Star Calibration Illustrating Gain Settings, Sky Reference, and Scintillation

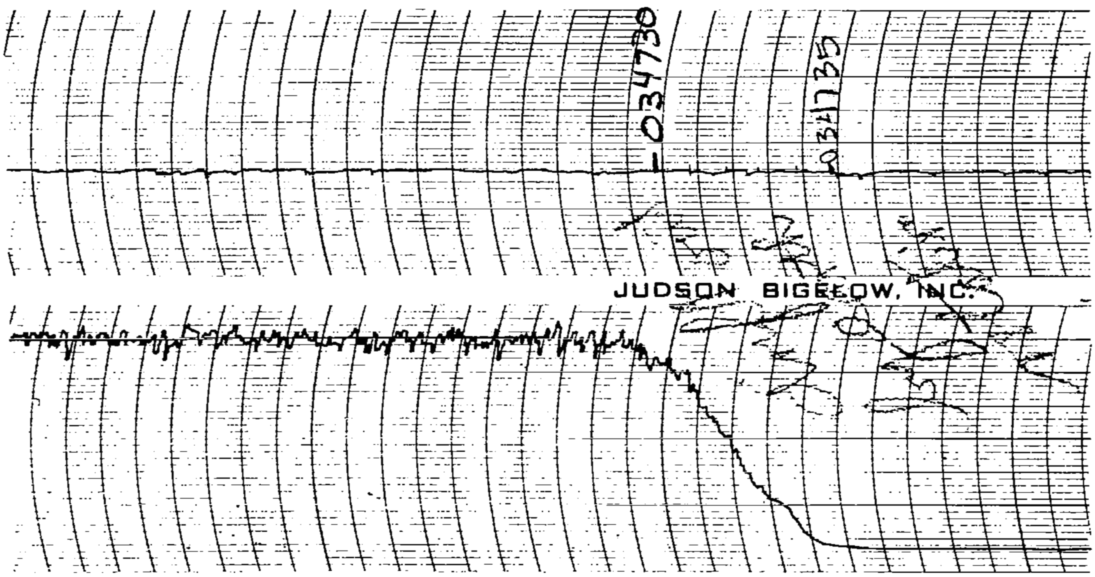

Figure 17. Star Drifting out of Field with Earth's Rotation

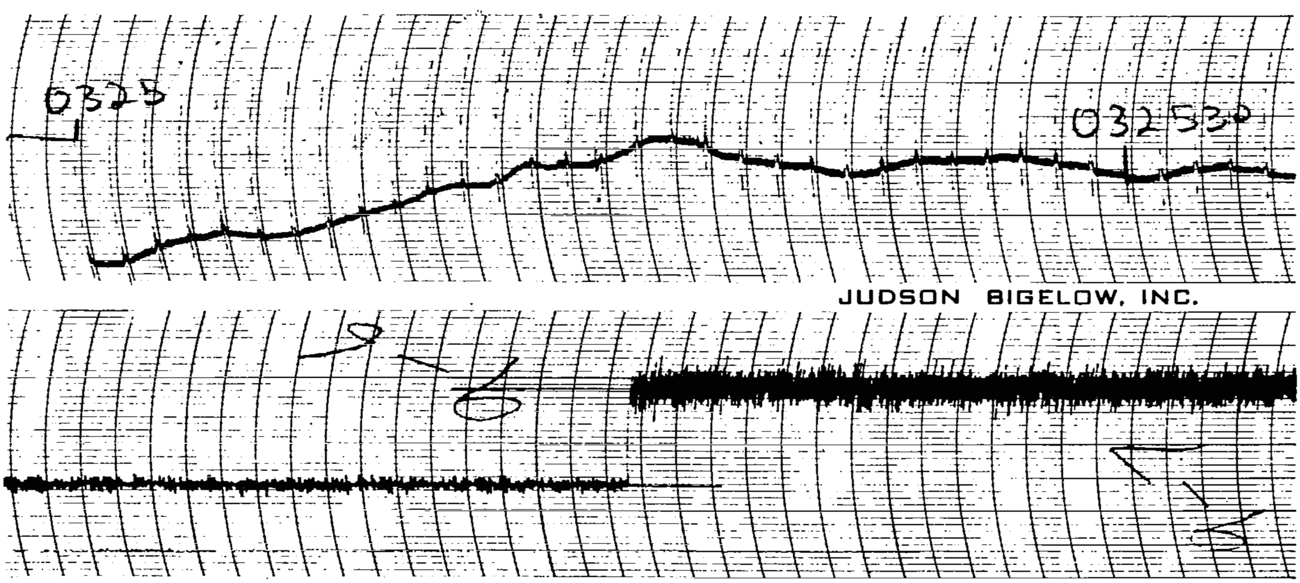

Figure 18. Gain Change (2. 5) with Radioactive Source

(4) Thin cloud errors: By continuous monitor of sky background.

(5) Limited utilization of data: By power spectral density reduction of data.

The method used in this program to minimize these effects was to utilize a number of runs and to process a relatively large number of points from each run to permit segregation of the data variations for the analytical purposes intended. Then the regression equations were applied to serve as a curve-fitting process according to the physical conditions involved.

C. ATMOSPHERIC EXTINCTION AND INSTRUMENT CALIBRATION

Photometric observations of identified first, second,and third magnitude stars in various parts of the sky were made before and/or after each observed Echo I pass for the purpose of calibration and extinction coefficient determination. The elevation of each star at the precise time of the calibration observation was then determined within 1/2 degree, utilizing its local hour angle and declination (Reference 9).

The visual extra-atmosphere magnitude of each reference star was then obtained from Reference 10. A separate investigation revealed that the star's color index had no significant effect upon the calibration.

For the visual photometer, a plot (Figure 19) of the raw calibration data on semi-log paper indicated that the instrument readings could be well fitted to the following regression equation:

$$m = a + b \log_{10} (IR) - kX,$$

where

m = the extra-atmosphere magnitude,

IR = instrument reading,

k = the extinction coefficient (1 atmosphere),

X = the effective number of atmospheres,

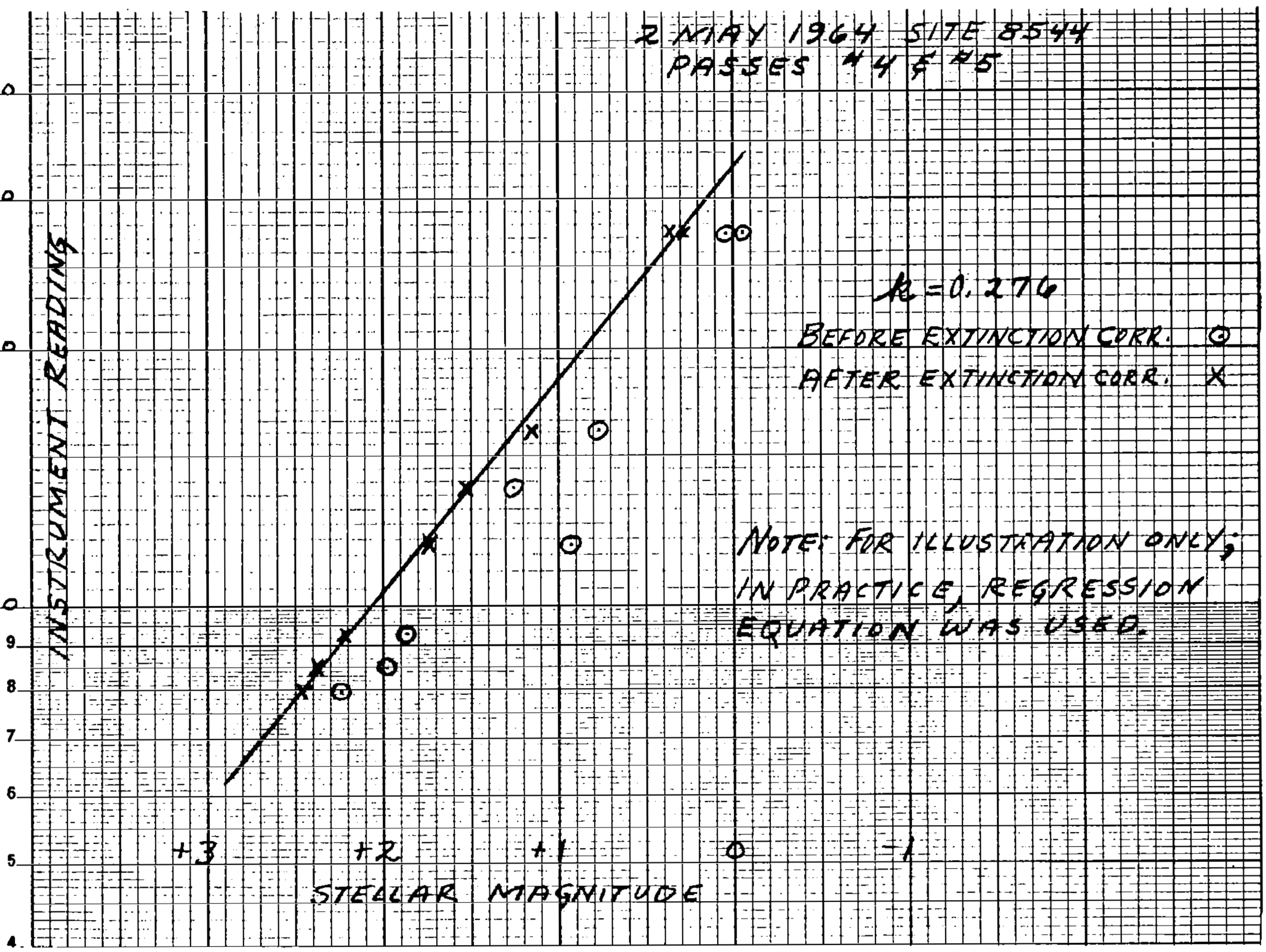

Figure 19. Visual Photometer Calibration Curve

$$= \sec z - 0.0018167 (\sec z - 1),$$
$$- 0.002875 (\sec z - 1)^2,$$
$$- 0.0008083 (\sec z - 1)^3 \text{ (Reference 9)},$$

and where z = zenith distance (90 deg - elevation).

Least-square best-fit solutions of this regression equation for a, b, and k were then performed for each of the calibrations. The results are presented in Table V.

The photoelectric calibrations were similarly fitted to the equation $m = a - 2.5 \log (IR) - kX$, and the results are given in Table VI.

D. COMPUTER PROCESSING AND ANALYSIS OF DATA

Data processing and analyses were highly automatized by the extensive use of the IBM 1410 computer. The calibration equations for both the visual and photoelectric photometers having been determined as described in the preceding section, the processing programs were written to assimilate the raw data.

This program was also used during the second observing "window" to generate the detailed pass predictions.

The processing program print-out is typified in Appendix I. The anomalistic orbital elements from the SAO acquisition Ephemeris VI are used in this program to determine the local look angles, slant range, and phase angle for each observation time. The elevation angle is used with the calibration equation to determine the satellite's stellar magnitude which is then reduced by the increment of magnitude due to earth albedo, as discussed in Section II. The resulting magnitude is then normalized to 1000 st mi and punched on cards, together with the phase angle, for use later in the analysis programs. If it were found, upon comparing the computed night ascensions and declinations with photographic tracking information during the observed pass, that more than a 3-second time error had accumulated,

Table V. Visual Photometer Calibrations and Atmosphere Extinction Determinations

$$m = a + b \log (IR) - kX$$

UT Date	For Pass No.	No. of Readings	No. of Elevations	No. of Stars	k	a	b	r	σ*	Site
3/1/64	0	39	18	17	0.207	6.446	-3.802	0.984	0.196	SAO Sta No. 8544
4/25/64	1,2	35	7	6	0.232	5.838	-3.705	0.932	0.231	
4/26/64	3	41	14	8	0.291	5.977	-3.952	0.960	0.245	
5/2/64	4,5	38	8	8	0.276	6.061	-3.987	0.985	0.139	
5/3/64	6,7	59	21	12	0.310	5.716	-3.649	0.934	0.326	
5/4/64	8,9	67	14	10	0.244	7.311	-4.614	0.951	0.238	
5/28/64	11	37	12	6	0.402	5.112	-3.710	0.952	0.278	GASPO (WFL)
5/30/64	13	54	16	12	0.153	5.289	-3.656	0.971	0.236	
6/5/64	17	18	7	7	0.377	6.526	-4.403	0.983	0.172	

*Standard deviations above 0.2 are associated with two or more calibration periods and are subject to the effect of changing extinction.

Table VI. Photoelectric Calibrations and Atmospheric Extinction Determinations

$$m + 2.5 \log IR = a - kX$$

UT Date	For Pass No.	No. of Readings	No. of Stars	k	a	r	σ	Site
5/30/64	13	55	6	0.209	5.340	0.955	0.111	GASPO (WFL)
6/5/64	17	51	12	0.403	5.630	0.843	0.224	

the mean anomaly equation of the orbital elements was adjusted and the program was rerun.

Pass 0 was reduced by a digital computer to the anomalistic orbital elements of Echo I provided by the SAO for acquisition Ephemeris VI, of epoch 3 March 1964, and required no correction.

Passes I through 9 were machine reduced to the anomalistic orbital elements of Echo I provided by SAO for acquisition Ephemeris VI, of epoch 28 April 1964, with the mean anomaly equation modified to read $M = 0.117147 + 12.573579 (t - t_0) + 3.107 \times 10^{-4} (t - t_0)^2$.

Passes 11 through 17 were machine reduced to the anomalistic orbital elements of Echo I provided by SAO for acquisition Ephemeris VI, of epoch 26 May 1964, and required no correction.

The machine analyses of the data first provided the A and B weighting coefficients for specular and diffuse reflection by best fitting the normalized data to Equation 4, and then determined the specularity in accordance with Equation 5. These results and other pertinent information are shown printed out in Appendix II for one typical pass (No. 13).

Next, having found B, the satellite's magnitude was adjusted by $-2.5 \log[2/3\ B\ F(\psi)]$ to eliminate the contribution of diffuse reflection, and the resulting "specular magnitude" was printed out for each observation. Utilizing the specular magnitude and an assumed coefficient of reflectivity of 0.83, the indicated radius of curvature at each observation is determined and printed out, together with their average radius of curvature.

A third machine analysis was a parametric solution of the reflectivity, based on the desired specular magnitudes. The print-out is also shown in Appendix II.

The original manually reduced "0 pass" results were used when applicable in confirming the machine processing and analysis programs.

SECTION V. RESULTS

Figures 20 through 30 present the normalized Echo I magnitudes versus phase angle for the selected passes, together with the results of each regression analysis. These passes were selected for a variety of considerations as those most suitable for yielding reliable, accurate data. A best-fit 100 percent diffuse curve was derived for each pass and is added to each graph to assist the reader in seeing clearly the data's departure from the diffuse theory.

Table VII summarizes the results of the several independent specularity determinations, showing for the visual photometry a probable error of less than 2 percent, determined in the manner prescribed by Reference 12.

The mean and extreme observed radii of curvature, assuming a reflectivity coefficient of 0. 83, are as follows:

	Mean R_c (ft)	Maximum R_c (ft)	Minimum R_c (ft)
Visual	51. 8	72. 1	33. 9
Photoelectric	48. 2	61. 2	39. 3

The parametric solutions for indicated coefficient of reflectivity are as follows:

R_c =	40	45	50	55	60 ft
Visual	1. 39	1. 10	0. 89	0. 74	0. 62
Photoelectric	1. 21	0. 95	0. 77	0. 64	0. 54

These results and local radii of curvature determinations for the visual observations are presented in Appendix III and for the photoelectric data in Appendix IV.

Table VII. Summarized Results of Echo I Photometric Studies on Contract No. NAS 1-3114

SPECULARITY DETERMINATIONS

Pass No.	No. of Measurements	$\frac{A}{A+B}$ * Ind % Specularity	Confidence Limits Probable Error	Confidence Limits .99 Level
Visual				
1, 2	32	99.7		
3	22	108.2		
4, 5	24	107.6		
6, 7	57	86.6		
8, 9	57	104.2		
11	13	92.4		
13	21	96.9		
17	11	100.0		
Accum	(237)	96.8	±1.8	±9.2
Photoelectric				
13	55	92.9		
17	51	100.8		
Accum	(106)	96.5		

*Reference 2 (Revised), 95.6 percent (18 points).

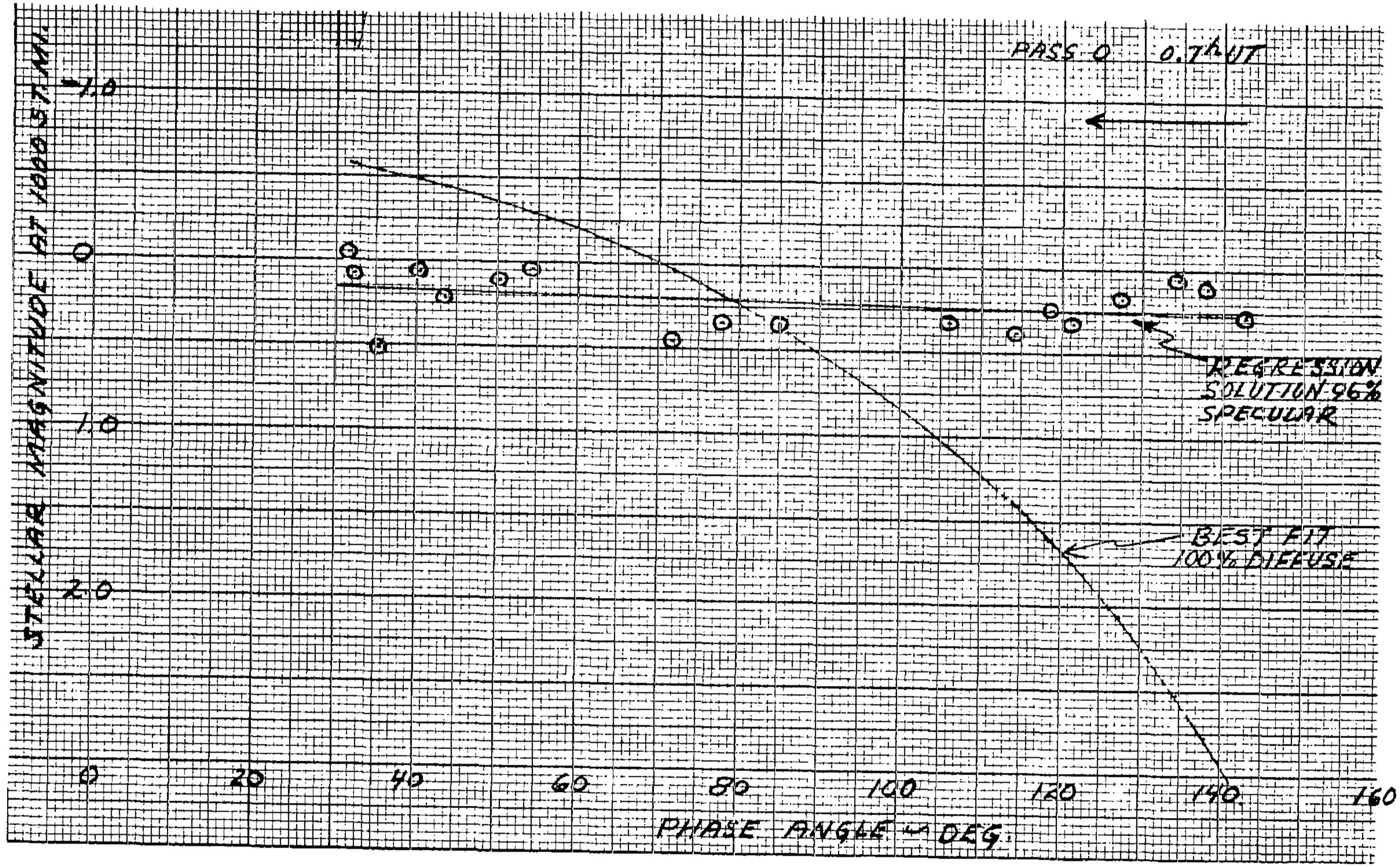

Figure 20. Regression Analysis (Visual) - Pass 0, 1 March 1964

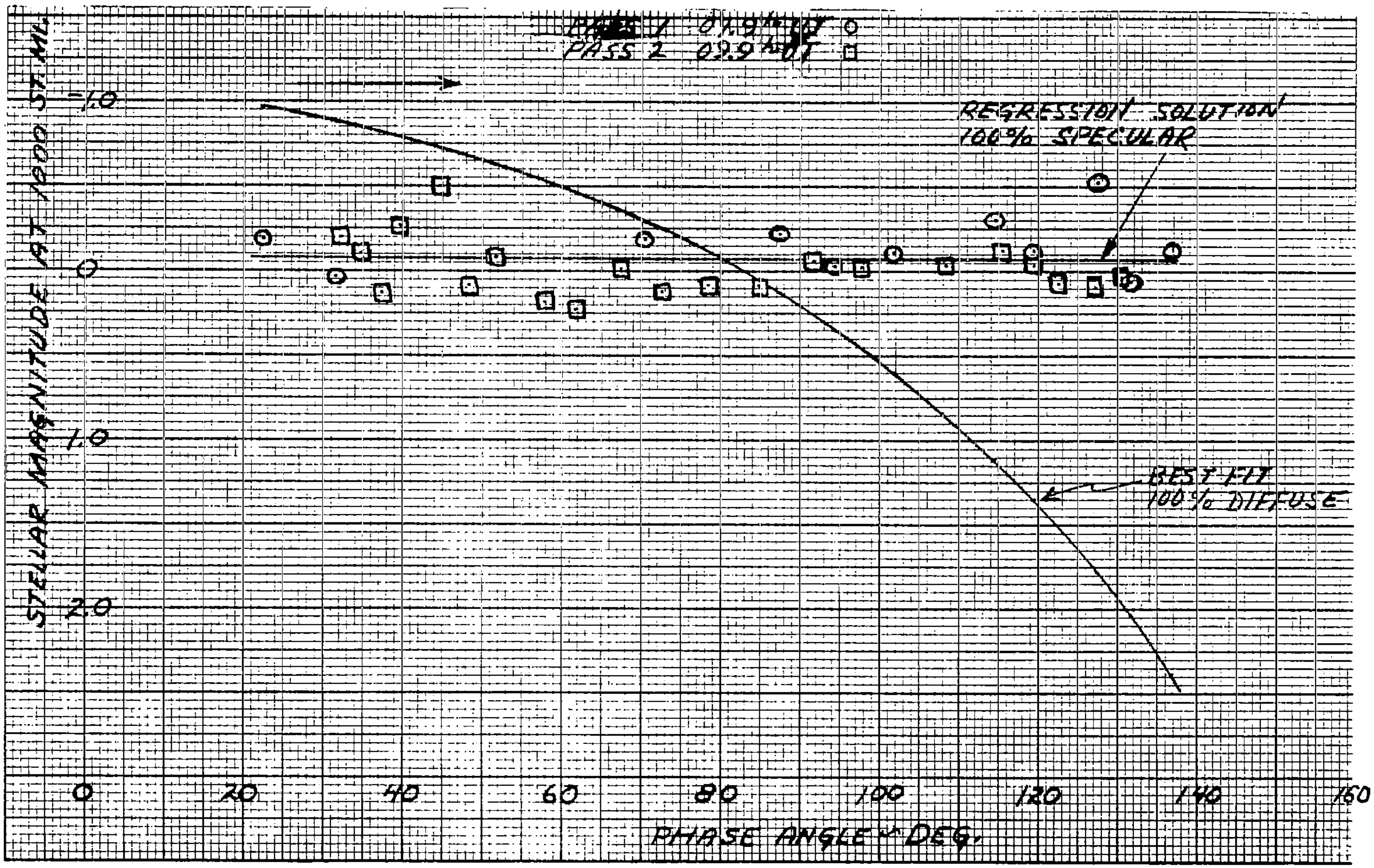

Figure 21. Regression Analysis (Visual) - Passes 1 and 2, 25 April 1964

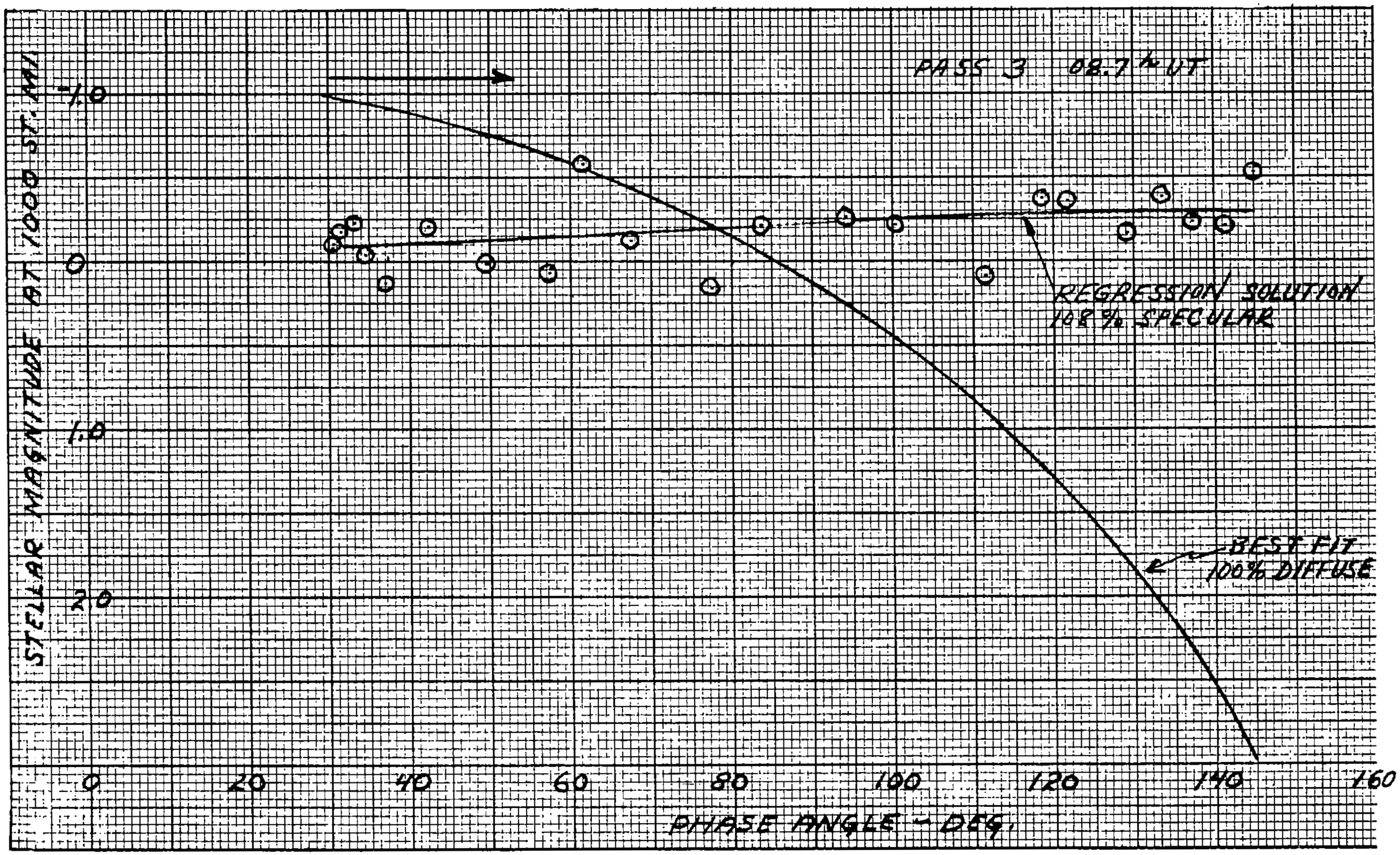

Figure 22. Regression Analysis (Visual) - Pass 3, 26 April 1964

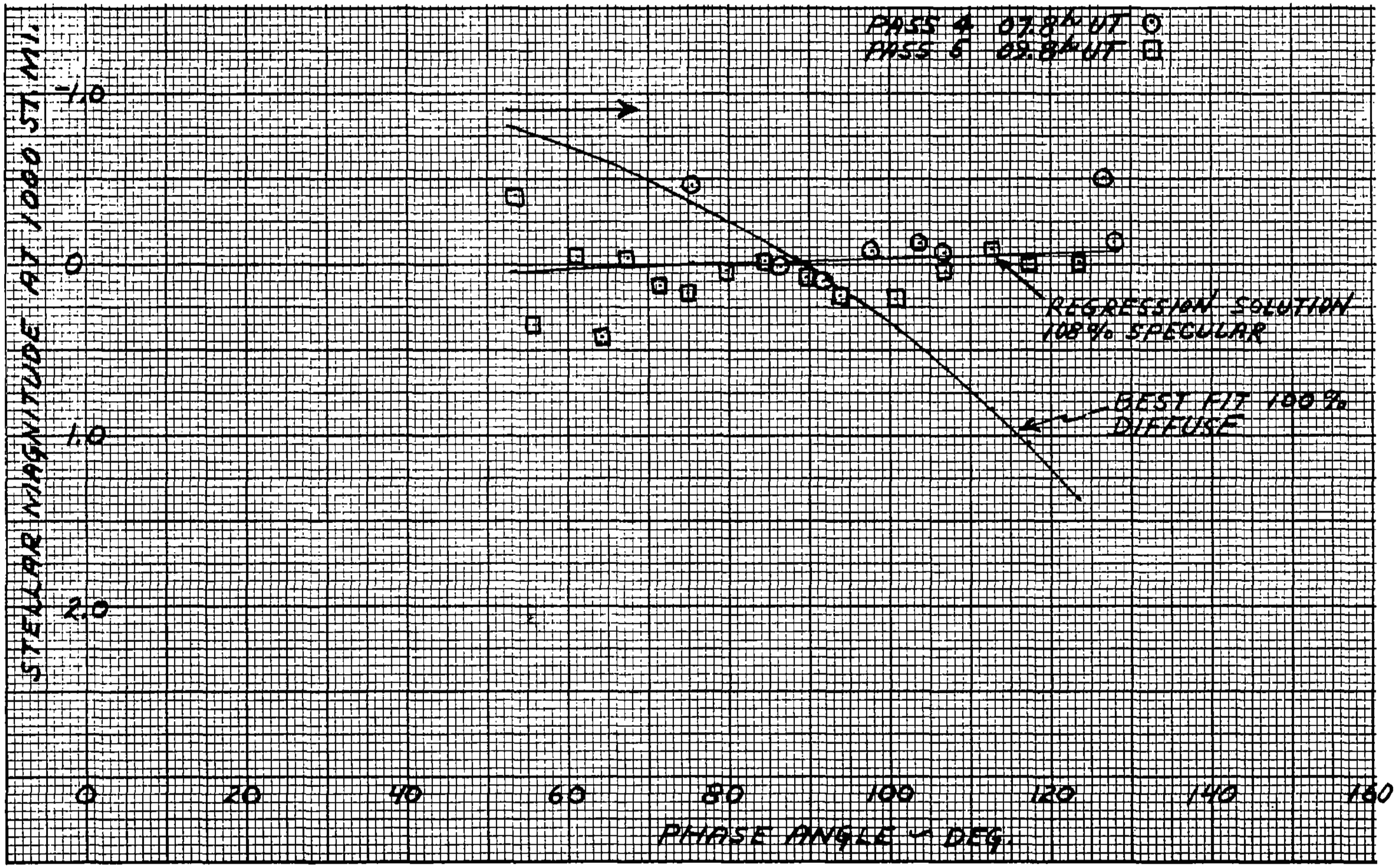

Figure 23. Regression Analysis (Visual) - Passes 4 and 5, 2 May 1964

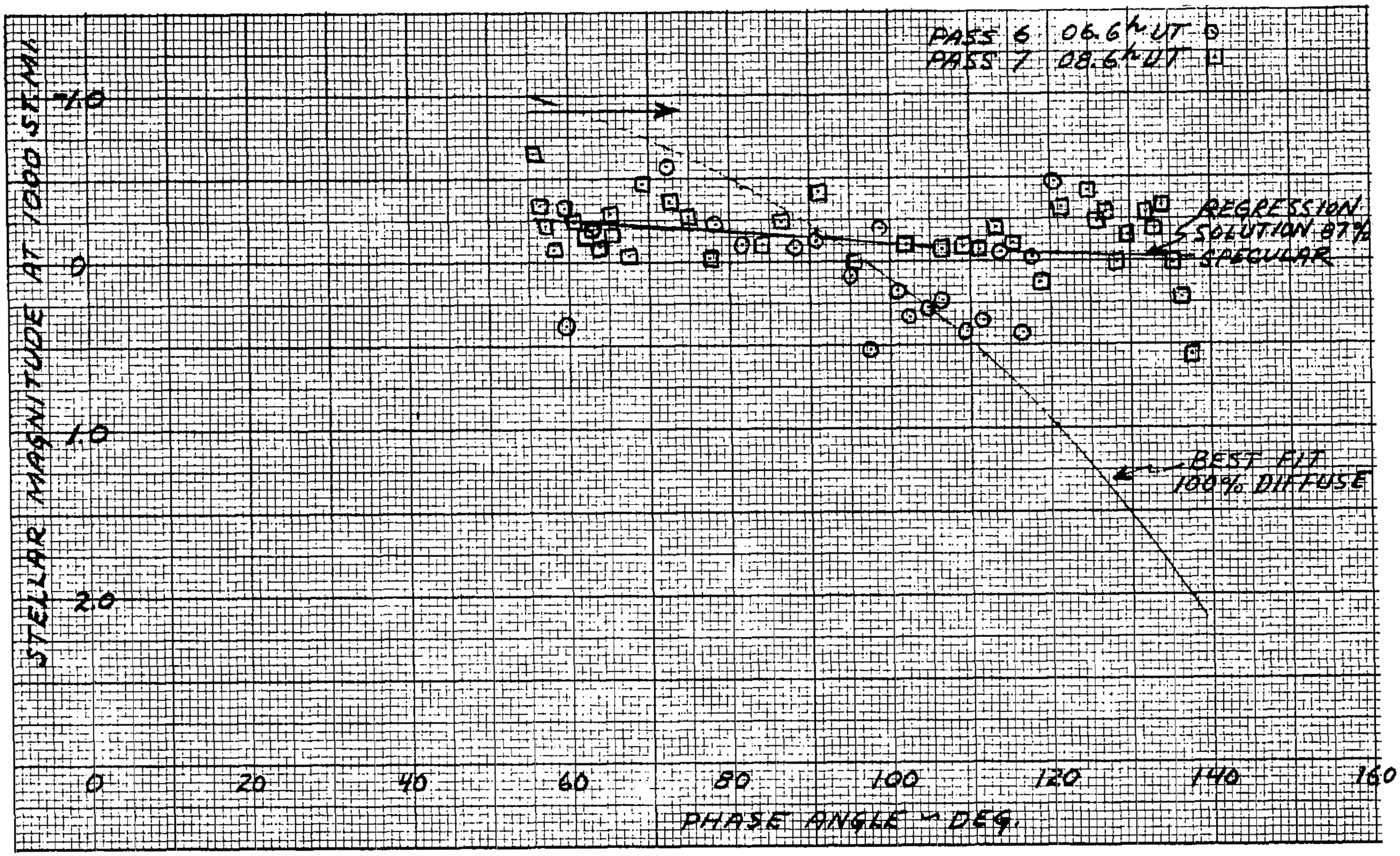

Figure 24. Regression Analysis (Visual) - Passes 6 and 7, 3 May 1964

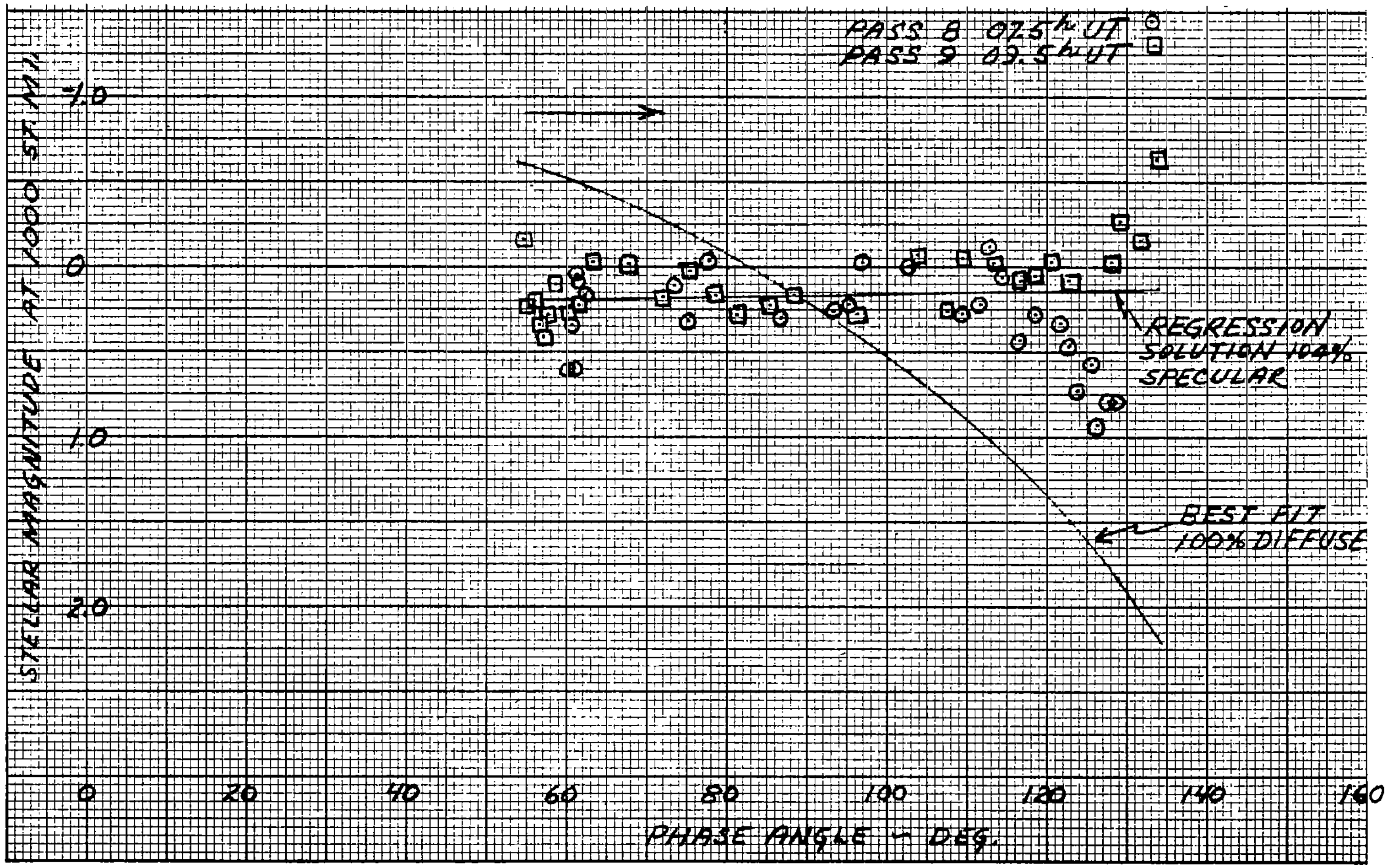

Figure 25. Regression Analysis (Visual) - Passes 8 and 9, 4 May 1964

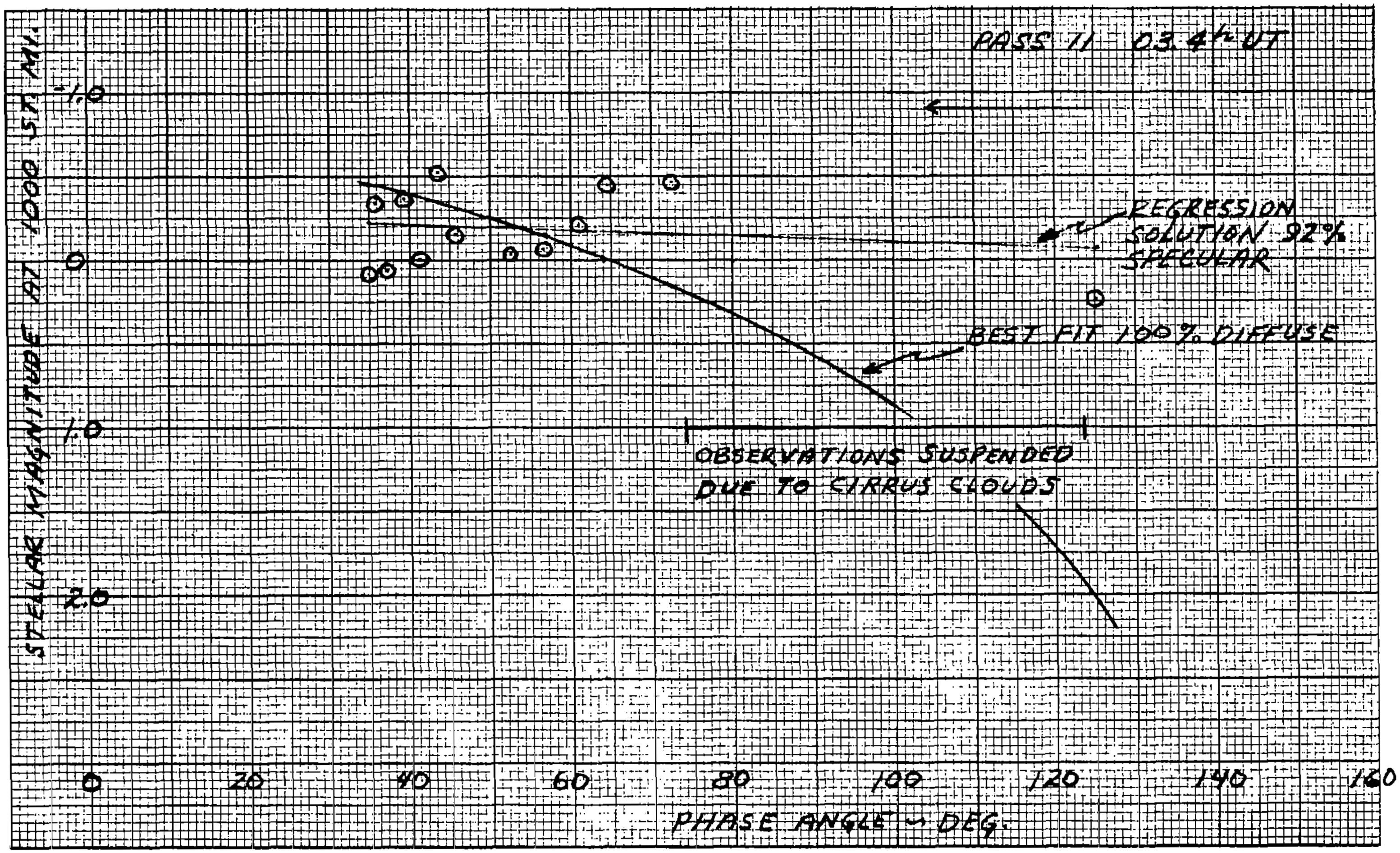

Figure 26. Regression Analysis (Visual) - Pass 11, 28 May 1964

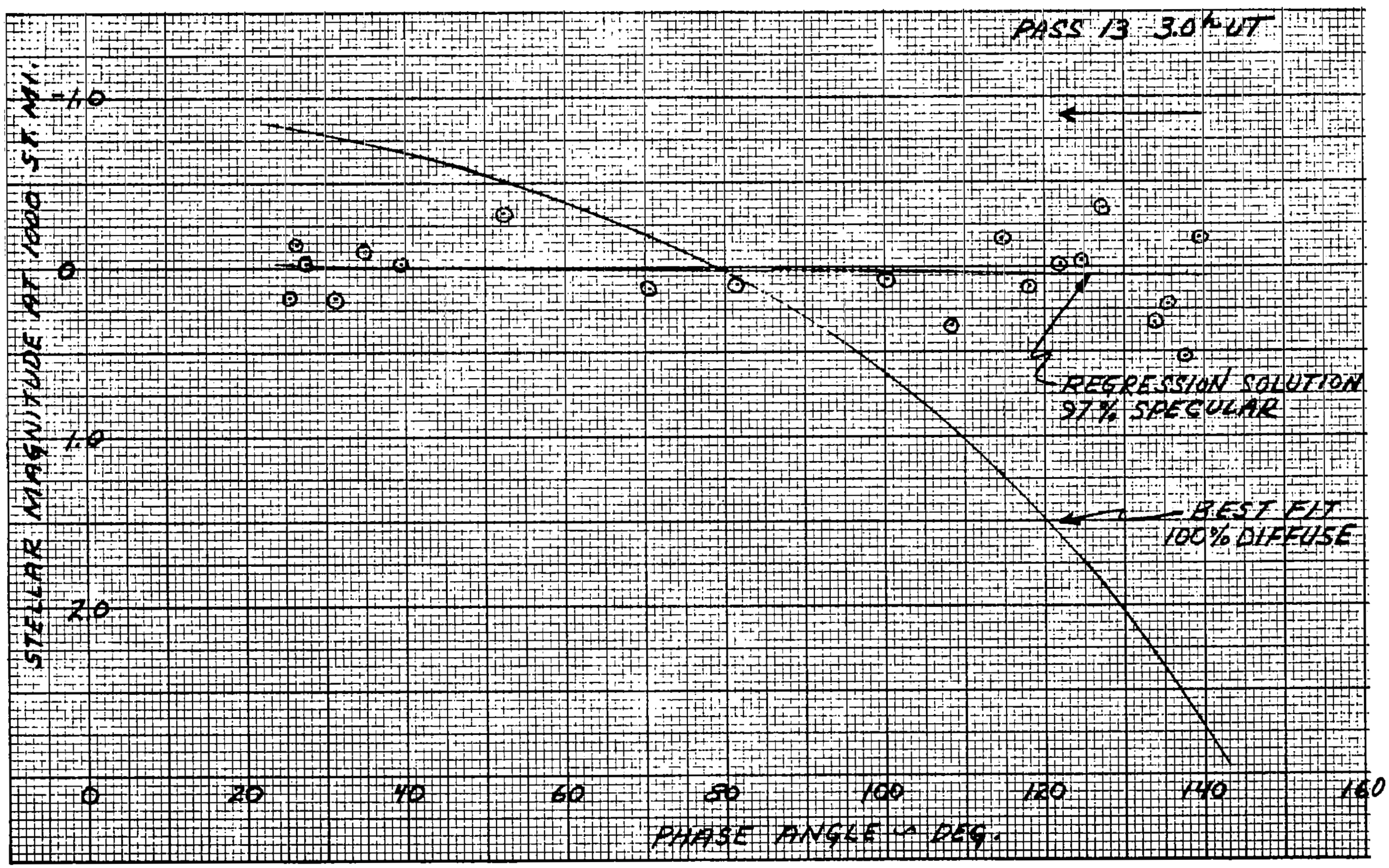

Figure 27. Regression Analysis (Visual) - Pass 13, 30 May 1964

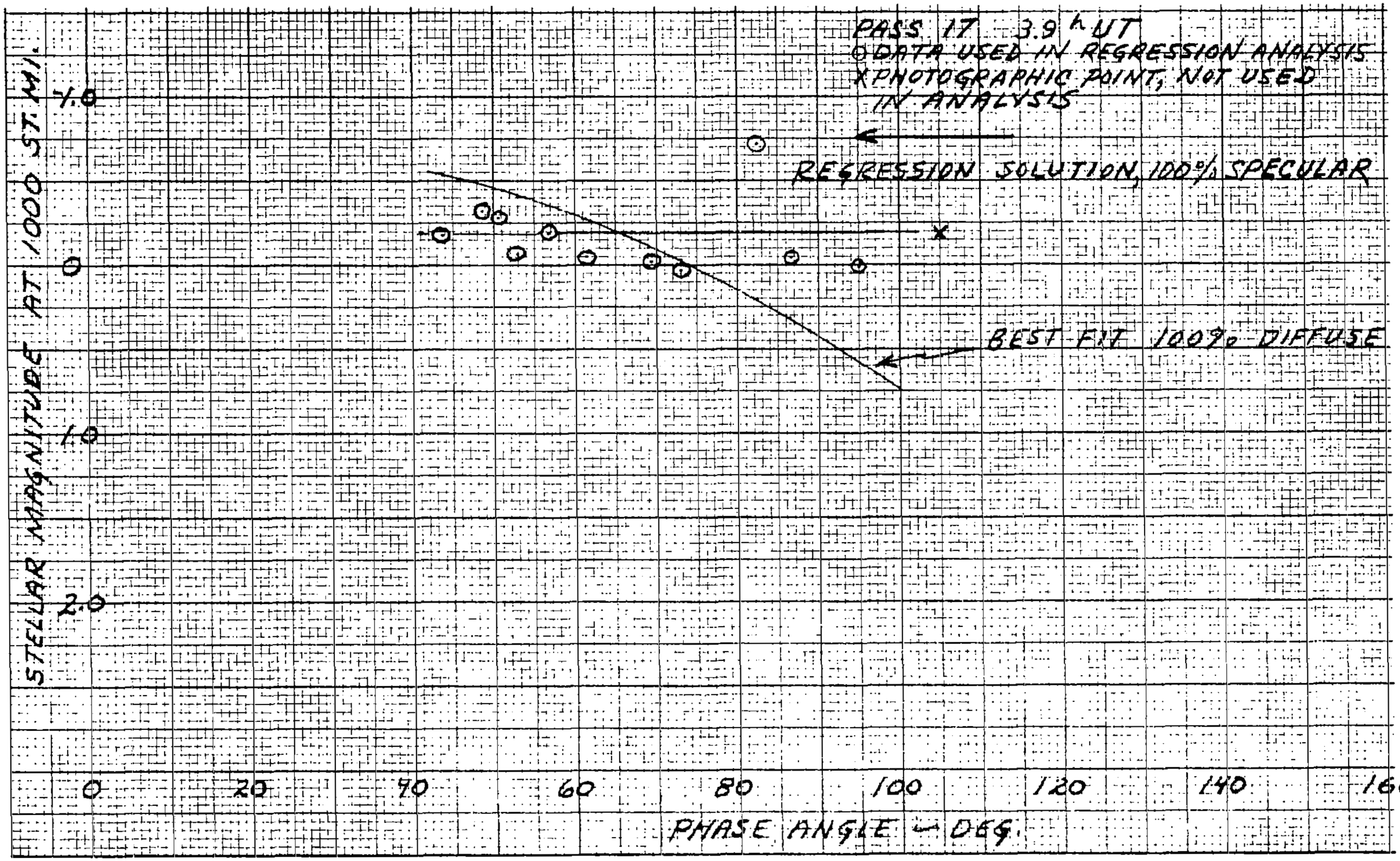

Figure 28. Regression Analysis (Visual) - Pass 17, 5 June 1964

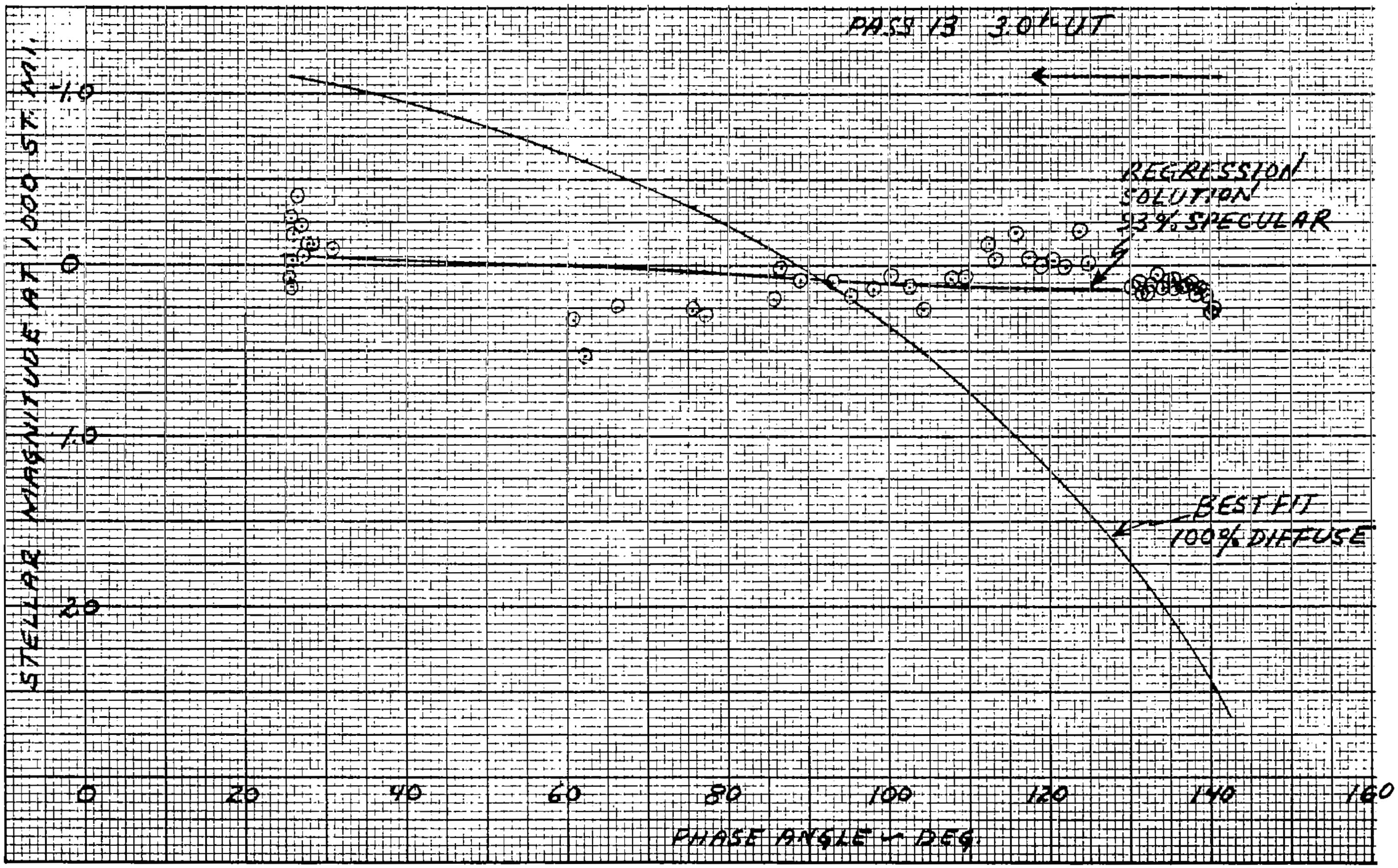

Figure 29. Regression Analysis (Photoelectric) - Pass 13, 30 May 1964

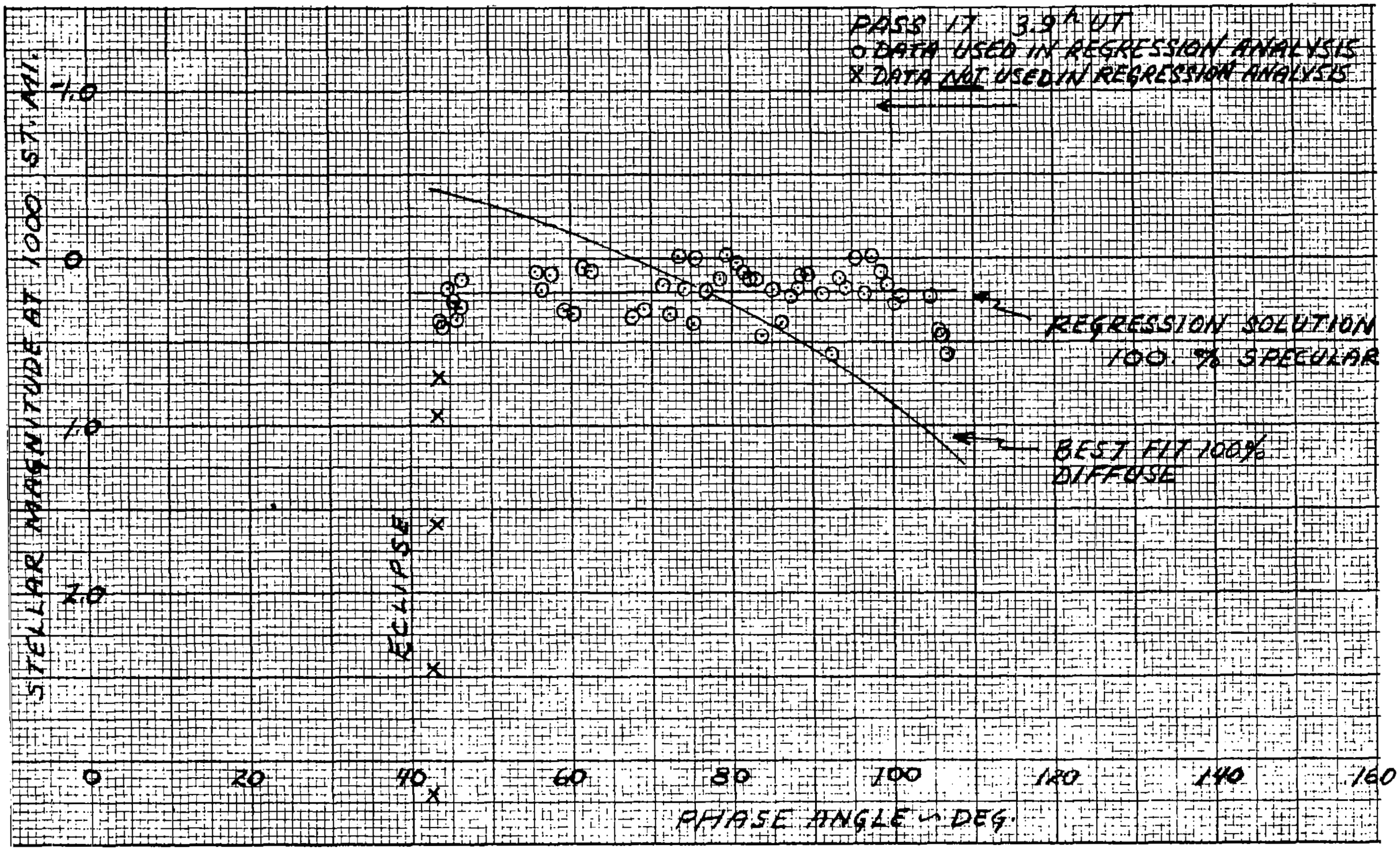

Figure 30. Regression Analysis (Photoelectric) - Pass 17, 5 June 1964

SECTION VI. CONCLUSIONS

The results of this program indicate the following about the Echo I satellite:

(1) Its present light reflection characteristic is highly specular as it was at the time of launch.

(2) Its mean radius of curvature remains near the design value, though local variations exist.

(3) Its total reflection coefficient is presently near the value at the time of launch.

These conclusions have certain engineering implications that include the following:

(1) The satellite environmental factors such as ultraviolet, solar wind, micrometeoroids, and hard vacuum have not removed or appreciably modified the reflectivity characteristics of the vapor-deposited aluminum.

(2) The forces such as solar pressure, meteorites, and thermal stresses resulting from the satellite passing in and out of the earth's shadow have not appreciably affected the satellite's over-all geometry.

(3) The space environment at the orbit of Echo I does not degrade aluminized Mylar optical surfaces as rapidly as feared in the more pessimistic estimates of the effects of satellite environments.

In addition, this program established new techniques of photometric observation and measurement that will prove valuable in various important applications utilizing optical signatures of space vehicles. The peripheral information gained in conducting this program indicates that a wide variety of scientific applications exist for these techniques.

SECTION VII. RECOMMENDATIONS

This program provided valuable information on the reflectivity characteristics of Echo I. However, much more information for use by astronautics engineers and space scientists can be provided utilizing similar but more comprehensive photometric observing and analysis techniques.

For example, Echo I could yield valuable additional information in the areas of (1) atmospheric light transmission characteristics by studying eclipse phenomena, (2) specifying passive satellite surface tolerances by relating its geometry determined by photometry to its microwave relay characteristics, (3) refining the effects of the space environment by monitoring its long-term time history of the degradation of its optical surfaces, and (4) determining effects of forces acting on an earth-satellite by obtaining a time history of its orientation.

Echo II should be observed for the same phenomena as Echo I. In addition, it may give valuable information on the effect of the space environment on its alodine thermal control coating through determining its optical color signature.

Both satellites can be used to refine the measurement and analysis techniques for obtaining the optical signatures of any earth satellite. Also, similar work could be done on other satellites.

Therefore, it is recommended that this program be extended and expanded to fully utilize the scientific knowledge that the existing Echo satellites and the techniques demonstrated can provide.

SECTION VIII. REFERENCES

1. The Echo Communications Satellite, IGY Bulletin 39, September 1960.

2. Emmons, R. H., An Indicated Specular Degradation Rate for Aluminized Mylar Surfaces in Near-Earth Orbit from Recent Photometric Observations of the Echo I Satellite, GER 11521, Goodyear Aerospace Corporation, Akron, Ohio, 26 March 1964. (Revised 17 June 1964)

3. Russell, H. N., Astrophysical Journal, Vol 43, 1916, p 173.

4. Tousey, R, "Optical Problems of the Satellite", Jr. Optical Society of America, Vol 47, 1957, p 261.

5. Tousey, R., "The Visibility of an Earth Satellite", Astronautic Acta, Vol 2, 1956.

6. Schneider, L. J., The Stellar Magnitude Increment of the Echo I Satellite due to the Earth's Albedo, Goodyear Memorandum SP-3225, 28 May 1964.

7. Ginter, R. L., Albedo Radiation on a Sphere or Planet-Oriented Flat Plate, GER 11618, Goodyear Aerospace Corporation, Akron, Ohio, June 1964.

8. Baker, Robert M. L., Jr., and Makemson, Maud W., An Introduction to Astrodynamics, Academic Press, New York, 1960, p 252.

9. Hardie, R. H., "Photoelectric Reductions", Ch. 8, Astronomical Techniques, Edited by W. A. Hiltner, Univ of Chicago Press, 1962.

10. MacRae, D. A., "The Brightest Stars," The Observers' Handbook, The Royal Astronomical Society of Canada, Toronto, 1964. (Based on H. L. Johnson and W. W. Morgan, The Astrophysical Journal, Vol 117, 1953, p 313.)

11. Veis, G., "Optical Tracking of Artificial Satellites", Space Science Reviews, II, D. Reidel Publ Co, Dordrecht, Holland, 1963, pp 250-296.

12. Wilks, S. S., Elementary Statistical Analysis, Princeton University Press, Princeton, N. J., 1951.

APPENDIX I

TYPICAL ORBITAL ELEMENT DATA

VISUAL PHOTOMETRY ECHO I NASA 013 WFL

YEAR	MO	DA	UT	HT	LONG	LAT	ALT	AZ	SR	RA	DEC	MAG	PHASE
1964	5	30	2 50 38.00	838.4	120.30	47.40	6.49	296.18	2295.5*	7 4.2	23.93		144.1
1964	5	30	2 51 38.00	852.6	115.83	47.49	10.65	296.40	2096.3*	7 18.4	26.84		141.1
1964	5	30	2 52 8.00	859.7	113.60	47.46	12.92	296.51	1998.4*	7 26.4	28.39	-0.173	139.3
1964	5	30	2 52 30.50	865.0	111.94	47.40	14.72	296.60	1925.8*	7 32.9	29.59		137.9
1964	5	30	2 52 37.00	866.6	111.46	47.38	15.25	296.62	1905.0*	7 34.9	29.94	0.527	137.5
1964	5	30	2 52 47.00	868.9	110.72	47.35	16.10	296.66	1873.1*	7 38.0	30.49		136.8
1964	5	30	2 53 5.00	873.2	109.40	47.27	17.66	296.72	1816.2*	7 43.9	31.51	0.217	135.6
1964	5	30	2 53 28.00	878.7	107.73	47.15	19.77	296.81	1744.5*	7 52.0	32.84	0.332	133.9
1964	5	30	2 53 30.00	879.2	107.58	47.13	19.96	296.82	1738.3*	7 52.7	32.96		133.7
1964	5	30	2 54 42.00	896.2	102.43	46.57	27.48	297.09	1523.3*	8 23.7	37.40	-0.349	127.4
1964	5	30	2 55 7.00	902.1	100.68	46.31	30.47	297.19	1452.8*	8 36.9	39.02	-0.031	124.8
1964	5	30	2 55 32.00	907.9	98.95	46.03	33.70	297.29	1384.9*	8 51.9	40.65	-0.014	122.0
1964	5	30	2 55 46.00	911.2	98.00	45.86	35.61	297.35	1348.3*	9 1.1	41.55		120.3
1964	5	30	2 56 3.00	915.2	96.85	45.64	38.06	297.42	1305.1*	9 13.1	42.64	0.112	118.1
1964	5	30	2 56 28.00	921.0	95.17	45.29	41.90	297.54	1244.7*	9 32.9	44.18	-0.171	114.7
1964	5	30	2 56 46.00	925.2	93.98	45.02	44.85	297.62	1203.9*	9 48.8	45.22		112.0
1964	5	30	2 57 9.00	930.5	92.49	44.66	48.87	297.74	1155.3*	10 11.3	46.39	0.341	108.4
1964	5	30	2 57 56.00	941.3	89.50	43.87	57.96	298.02	1070.6*	11 4.8	47.97	0.067	100.2
1964	5	30	2 58 26.00	948.1	87.65	43.31	64.37	298.26	1028.5*	11 43.7	48.11		94.3
1964	5	30	2 59 26.00	961.5	84.07	42.11	78.31	299.30	977.6*	13 5.3	45.66	0.097	81.6
1964	5	30	2 59 59.00	968.8	82.18	41.40	86.32	302.80	970.3*	13 47.6	42.74		74.4
1964	5	30	3 0 16.00	972.6	81.22	41.03	89.44	84.20	972.6*	14 7.7	40.88	0.125	70.6
1964	5	30	3 0 40.00	977.8	79.89	40.48	83.74	115.10	982.6*	14 33.9	37.94		65.5
1964	5	30	3 0 59.00	981.9	78.86	40.03	79.27	116.36	996.0*	14 52.6	35.44		61.5
1964	5	30	3 1 12.00	984.6	78.16	39.72	76.29	116.77	1007.9*	15 4.5	33.66		58.9
1964	5	30	3 1 26.00	987.6	77.42	39.38	73.15	117.06	1023.0*	15 16.5	31.73		56.2
1964	5	30	3 1 47.00	992.1	76.32	38.86	68.62	117.36	1050.0*	15 33.0	28.81	-0.322	52.3
1964	5	30	3 2 3.00	995.4	75.50	38.46	65.31	117.52	1073.8*	15 44.4	26.61		49.5
1964	5	30	3 2 40.00	1003.1	73.64	37.51	58.19	117.80	1138.4*	16 7.6	21.69		43.7
1964	5	30	3 3 11.00	1009.4	72.12	36.68	52.79	117.98	1201.5*	16 24.1	17.82	-0.018	39.6
1964	5	30	3 3 31.00	1013.4	71.16	36.14	49.57	118.08	1245.9*	16 33.6	15.47	0.031	37.3
1964	5	30	3 3 40.00	1015.2	70.74	35.89	48.19	118.12	1266.7*	16 37.7	14.45		36.3
1964	5	30	3 3 53.00	1017.8	70.13	35.53	46.26	118.17	1297.6*	16 43.2	13.02	-0.103	35.0
1964	5	30	3 4 40.00	1026.9	67.98	34.21	39.89	118.36	1416.6*	17 1.2	8.25	0.174	31.1
1964	5	30	3 5 41.00	1038.4	65.32	32.44	32.88	118.58	1584.2*	17 20.5	2.92	-0.026	27.8
1964	5	30	3 6 19.00	1045.4	63.72	31.30	29.09	118.70	1694.1*	17 30.9	0.01	-0.141	26.6
1964	5	30	3 6 45.00	1050.0	62.66	30.51	26.70	118.78	1771.1*	17 37.5	-1.82		26.1
1964	5	30	3 7 16.00	1055.4	61.42	29.56	24.06	118.88	1864.5*	17 44.8	-3.85		25.8
1964	5	30	3 7 17.00	1055.6	61.38	29.53	23.97	118.88	1867.6*	17 45.0	-3.92		25.8
1964	5	30	3 7 18.00	1055.8	61.34	29.50	23.89	118.88	1870.6*	17 45.2	-3.98		25.8
1964	5	30	3 7 19.50	1056.0	61.28	29.45	23.77	118.89	1875.2*	17 45.6	-4.07		25.8
1964	5	30	3 7 33.00	1058.4	60.75	29.04	22.69	118.93	1916.4*	17 48.6	-4.91	0.181	25.7
1964	5	30	3 7 40.00	1059.5	60.48	28.82	22.14	118.95	1937.9	17 50.1	-5.33		25.7

APPENDIX II

TYPICAL RESULTS OF COMPUTER DATA REDUCTION

VISUAL PHOTOMETRY ECHO I NASA 013 WFL

21 POINTS

MEAN MAGNITUDE 0.04081

SIGMA OF THE MAGNITUDES IS 0.21158

CORRELATION COEF. IS 0.15308

STUDENTS T IS 0.70150

MAGNITUDE FOR B # 0 IS, 0.02049

ASSUMED COEF. OF REFLECTIVITY 0.83000

REGRESSION A IS 3.78956

REGRESSION B IS 0.12222

SPECULARITY FROM REGRESSION 0.96876

VISUAL PHOTOMETRY ECHO I NASA 013 WFL

I	MAGNITUDE	ANGLE	MAG. A#0	MSP	RADIUS
1	-0.17292	139.33871	2.67664	-0.17020	56.50673
2	0.52743	137.50490	2.53808	0.53333	40.86898
3	0.21747	135.57160	2.39882	0.22251	47.15828
4	0.33177	133.85040	2.28027	0.33802	44.71528
5	-0.34893	127.35389	1.87297	-0.34407	61.21741
6	-0.03145	124.77015	1.72638	-0.02399	52.82737
7	-0.01360	121.95255	1.57517	-0.00488	52.36446
8	0.11163	118.10464	1.38188	0.12334	49.36202
9	-0.17127	114.68365	1.22158	-0.16082	56.26315
10	0.34118	108.41589	0.95274	0.36276	44.20888
11	0.06747	100.17035	0.64117	0.08982	50.12990
12	0.09724	81.63482	0.07891	0.13609	49.07306
13	0.12455	70.64583	-0.18220	0.17550	48.19044
14	-0.32173	52.31017	-0.52135	-0.27567	59.31914
15	-0.01756	39.60106	-0.69417	0.05477	50.94561
16	0.03072	37.25996	-0.72081	0.10841	49.70263
17	-0.10339	34.98062	-0.74524	-0.03341	53.05710
18	0.17434	31.08615	-0.78352	0.26901	46.15917
19	-0.02616	27.80003	-0.81245	0.05415	50.96016
20	-0.14058	26.60744	-0.82219	-0.06790	53.90655
21	0.18079	25.73860	-0.82903	0.28032	45.91936

MEAN RADIUS IS 50.37136 MEAN SPECULAR MAG IS 0.07939

RADIUS	INDICATED REFLECTIVITY
40	1.3162121
45	1.0399699
50	0.8423758
55	0.6961785
60	0.5849832

APPENDIX III

CUMULATIVE RESULTS OF ECHO I VISUAL COMPARISON PHOTOMETRY

CUMULATIVE VISUAL PHOTOMETRY ECHO I NASA [redacted] [redacted] INVESTIGATOR R.H. EMMONS

237 POINTS 12 PASSES, NO. 1, 2, 3, 4, 5, 6, 7, 8, 9, 11, 13, 17 RHE 6/18/64

MEAN MAGNITUDE -0.01812

SIGMA OF THE MAGNITUDES IS 0.27179

CORRELATION COEF. IS 0.09016

STUDENTS T IS 1.38798

MAGNITUDE FOR B # 0 IS, -0.05128

COEF. OF REFLECTIVITY 0.83000 ← ASSUMED FOR RADIUS OF CURVATURE DETERMINATIONS

REGRESSION A IS 4.05991

REGRESSION B IS 0.13217

SPECULAR ITY [redacted] FROM REGRESSION 0.96847 = 96.8% PROBABLE ERROR ± 01.9% (FROM VISUAL ONLY)

AT .99 CONFIDENCE LEVEL SPECULARITY LIES BETWEEN 87.6% and 106%

237 VISUAL POINTS

PARAMETRIC SOLUTION

RADIUS	INDICATED REFLECTIVITY
40	1.3918761
45	1.0997538
50	0.8908008
55	0.7361991
60	0.6186116

(45, 50) COMPARE WITH INDEPENDENT 1 VISUAL PASS 3/1/64 BY GAC: 95.6%

COMPARE WITH INDEPENDENT PHOTOELECTRIC 2 PASSES: 96.5%

I	MAGNITUDE	ANGLE	MAG. A#0	MSP	RADIUS
1	-0.19410	22.22898	-1.02814	-0.11687	55.13592
2	0.02506	31.50084	-0.95332	0.11373	49.58091
3	-0.19748	70.37844	-0.36165	-0.15649	56.15120
4	-0.21345	87.25086	0.05800	-0.18618	56.92418
5	-0.03487	94.36310	0.27264	-0.00850	52.45188
6	-0.11243	101.70537	0.52223	-0.09298	54.53275
7	-0.30458	114.54914	1.04181	-0.29453	59.83651
8	-0.12685	119.39347	1.27135	-0.11727	55.14603
9	-0.52153	127.37567	1.70057	-0.51705	66.29360
10	0.05096	131.64829	1.96179	0.05693	50.89504
11	-0.13777	136.85309	2.31670	-0.13416	55.57664
12	-0.20454	32.10863	-0.94756	-0.13373	55.56562
13	-0.10713	34.76629	-0.92113	-0.03136	53.00701
14	0.11765	37.30425	-0.89399	0.20920	47.44832
15	-0.26752	39.76889	-0.86587	-0.20580	57.44076
16	-0.50182	44.77369	-0.80331	-0.45519	64.43142
17	0.07789	48.35436	-0.75400	0.15496	48.64837
18	-0.08602	51.63628	-0.70541	-0.02305	52.80457
19	0.17745	57.85644	-0.60415	0.25091	46.54555
20	0.22441	61.80451	-0.53343	0.29623	45.58425
21	-0.02248	67.29016	-0.42649	0.02888	51.55658
22	0.11811	72.53083	-0.31440	0.17087	48.29321
23	0.08122	78.42167	-0.17607	0.12596	49.30258
24	0.08757	84.75478	-0.01162	0.12613	49.29852
25	-0.05774	91.62015	0.18689	-0.02978	52.96836
26	-0.02193	97.77228	0.38475	0.00211	52.19616
27	-0.03858	108.31756	0.77508	-0.02211	52.78166
28	-0.12454	115.35041	1.07835	-0.11306	55.03926
29	-0.04189	119.41052	1.27219	-0.03153	53.01114
30	0.07063	122.51853	1.43119	0.08055	50.34431
31	0.09273	127.08512	1.68368	0.10075	49.87825
32	0.03051	130.54052	1.89166	0.03676	51.36999
33	-0.10585	30.47938	-0.96276	-0.02691	52.89851
34	-0.18159	31.50199	-0.95331	-0.10882	54.93179
35	-0.23848	33.05925	-0.93834	-0.17052	56.51500
36	-0.04004	34.75395	-0.92125	0.04075	51.27558
37	0.12585	37.04113	-0.89689	0.21838	47.24810
38	-0.21023	42.25949	-0.83565	-0.14690	55.90378
39	0.00805	49.84032	-0.73241	0.07869	50.38749
40	0.06798	57.63811	-0.60791	0.13441	49.11090
41	-0.58176	61.69127	-0.53553	-0.54811	67.24839
42	-0.12646	67.52392	-0.42170	-0.08010	54.21013
43	0.15640	77.48236	-0.19904	0.20546	47.52999
44	-0.22169	83.75911	-0.03861	-0.19208	57.07893
45	-0.26957	94.24199	0.26877	-0.24830	58.57619
46	-0.22184	100.40606	0.47581	-0.20350	57.37999
47	0.08871	111.57624	0.91084	0.10505	49.77954
48	-0.37974	118.71656	1.23799	-0.37192	62.00752
49	-0.36061	121.77287	1.39215	-0.35371	61.48964
50	-0.17309	129.16708	1.80711	-0.16749	56.43643
51	-0.38584	133.58449	2.08871	-0.38229	62.30452
52	-0.24140	137.28359	2.34812	-0.23821	58.30461
53	-0.20993	141.32565	2.66087	-0.20747	57.48502
54	-0.53577	144.96337	2.97365	-0.53440	66.82539
55	-0.46655	75.44712	-0.24761	-0.43791	63.92091
56	0.00551	86.51569	0.03720	0.03963	51.30216
57	0.09784	91.81061	0.19272	0.13000	49.21089

58	-0.07451	97.80491	0.38585	-0.05164	53.50433
59	-0.12350	103.74524	0.59720	-0.10555	54.84919
60	-0.06997	106.86981	0.71723	-0.05309	53.54010
61	-0.50620	126.62634	1.65721	-0.50147	65.81966
62	-0.13926	128.04421	1.73985	-0.13312	55.55000
63	-0.40278	53.38557	-0.67816	-0.35728	61.59083
64	0.35086	55.69601	-0.64070	0.44066	42.65094
65	-0.05225	61.13150	-0.54585	0.00365	52.15925
66	0.41160	64.22182	-0.48758	0.49379	41.62005
67	-0.03967	67.48769	-0.42244	0.01068	51.99070
68	0.11564	71.53080	-0.33656	0.16939	48.32614
69	0.16226	74.99518	-0.25817	0.21443	47.33427
70	0.02727	79.66022	-0.14523	0.06858	50.62264
71	-0.02632	84.49848	-0.01861	0.00857	52.04115
72	0.06849	89.81339	0.13248	0.10159	49.85891
73	0.18257	93.88277	0.25735	0.21534	47.31438
74	0.19659	100.83184	0.49091	0.22328	47.14155
75	0.04493	106.95047	0.72041	0.06365	50.73763
76	-0.09654	112.62628	0.95629	-0.08335	54.29130
77	-0.00218	117.12496	1.16124	0.00973	52.01339
78	-0.02095	123.51395	1.48423	-0.01227	52.54300
79	0.38214	59.70850	-0.57161	0.46874	42.10295
80	-0.18955	62.41993	-0.52194	-0.14154	55.76587
81	-0.57314	72.16774	-0.32249	-0.54534	67.16265
82	-0.23329	78.34976	-0.17784	-0.19992	57.28563
83	-0.10492	81.38443	-0.10125	-0.06990	53.95607
84	-0.08785	88.16733	0.08428	-0.05793	53.65955
85	-0.13311	90.69978	0.15898	-0.10636	54.86971
86	0.08213	95.13832	0.29758	0.11086	49.64646
87	0.51727	97.53037	0.37658	0.55736	40.41921
88	-0.20332	98.80911	0.42012	-0.18367	56.85841
89	0.16818	100.90380	0.49347	0.19411	47.77907
90	0.33234	102.39432	0.54726	0.36109	44.24288
91	0.26915	104.88448	0.64022	0.29400	45.63104
92	0.23296	106.55202	0.70472	0.25559	46.44546
93	0.40970	109.73840	0.83331	0.43336	42.79449
94	0.34856	111.60612	0.91212	0.36934	44.07513
95	-0.05744	113.87559	1.01151	-0.04444	53.32727
96	0.41887	116.46597	1.13014	0.43698	42.72329
97	-0.03344	117.78840	1.19295	-0.02221	52.78397
98	-0.48416	120.71562	1.33777	-0.47768	65.10245
99	-0.65203	55.62623	-0.64186	-0.61722	69.42323
100	-0.34616	56.24119	-0.63162	-0.30022	59.99368
101	-0.22270	56.98905	-0.61900	-0.17171	56.54606
102	-0.08069	58.04353	-0.60091	-0.02337	52.81220
103	-0.33500	59.50703	-0.57520	-0.29098	59.73876
104	-0.24427	60.79161	-0.55206	-0.19736	57.21795
105	-0.16298	62.24976	-0.52513	-0.11360	55.05306
106	-0.09680	63.94079	-0.49301	-0.04581	53.36092
107	-0.29463	65.16464	-0.46915	-0.25324	58.70958
108	-0.04606	67.49943	-0.42220	0.00397	52.15146
109	-0.47807	69.11009	-0.38869	-0.44575	64.15197
110	-0.36795	72.53831	-0.31423	-0.33453	60.94904
111	-0.27266	75.02277	-0.25753	-0.23801	58.29926
112	-0.02972	77.48199	-0.19905	0.01147	51.97174
113	-0.10362	84.05000	-0.03077	-0.07079	53.97832
114	-0.24211	86.71745	0.04288	-0.21518	57.68955
115	-0.43146	91.08828	0.17071	-0.41142	63.14576
116	0.00649	95.52831	0.31025	0.03295	51.46011
117	-0.11066	102.03501	0.53417	-0.09140	54.49290
118	-0.07970	106.45271	0.70083	-0.06272	53.77795
119	-0.09682	109.06615	0.80558	-0.08165	54.24895
120	-0.07044	111.13629	0.89205	-0.05610	53.61419
121	-0.20367	113.12136	0.97802	-0.19196	57.07593
122	-0.11217	115.21215	1.07201	-0.10049	54.72157
123	0.12314	118.61550	1.23305	0.13565	49.08290

124	-0.32429	121.43665	1.37473	-0.31703	60.45993
125	-0.42105	124.80772	1.55478	-0.41543	63.26260
126	-0.24475	125.86740	1.61399	-0.23849	58.31210
127	-0.30218	126.99430	1.67842	-0.29659	59.89326
128	0.00735	128.16900	1.74724	0.01434	51.90311
129	-0.16210	129.94033	1.85440	-0.15669	56.15629
130	-0.29574	131.96680	1.98228	-0.29149	59.75284
131	-0.19968	133.13228	2.05855	-0.19535	57.16509
132	-0.33866	133.93509	2.11231	-0.33504	60.96323
133	0.00778	135.30601	2.20653	0.01235	51.95054
134	0.21405	136.18364	2.26851	0.21927	47.22868
135	0.55708	137.56494	2.36884	0.56362	40.30298
136	0.60389	60.03189	-0.56581	0.71051	37.66675
137	0.34122	60.39619	-0.55924	0.42351	42.98909
138	0.59393	60.77381	-0.55239	0.69817	37.88149
139	0.03868	61.14351	-0.54563	0.09959	49.90492
140	0.08047	61.70923	-0.53520	0.14321	48.91228
141	0.15882	62.33288	-0.52358	0.22567	47.08986
142	0.10386	73.41903	-0.29440	0.15495	48.64874
143	0.31471	75.09558	-0.25583	0.37483	43.96379
144	-0.04315	77.93120	-0.18811	-0.00289	52.31660
145	0.29637	86.84559	0.04650	0.34079	44.65827
146	0.25441	93.27237	0.23808	0.29009	45.71325
147	0.21493	95.19490	0.29941	0.24740	46.62087
148	-0.02568	96.97195	0.35786	-0.00112	52.27376
149	-0.00867	102.69026	0.55810	0.01204	51.95796
150	0.26253	109.52681	0.82455	0.28333	45.85575
151	0.20728	111.75990	0.91872	0.22539	47.09592
152	-0.12601	112.94806	0.97039	-0.11334	55.04637
153	0.05814	114.34110	1.03241	0.07233	50.53532
154	0.42121	116.66832	1.13965	0.43920	42.67963
155	0.27869	118.50425	1.22762	0.29322	45.64755
156	0.33454	121.84587	1.39594	0.34763	44.51795
157	0.46269	122.70537	1.44106	0.47653	41.94650
158	0.72582	123.75779	1.49738	0.74294	37.10837
159	0.56669	125.17598	1.57521	0.58044	39.99205
160	0.92270	126.23723	1.63497	0.94079	33.87677 ← MIN. OBSERVED
161	0.79779	127.70096	1.71961	0.81269	35.93549
162	0.78603	128.74441	1.78160	0.79994	36.14701
163	-0.16069	54.83214	-0.65490	-0.10476	54.82931
164	0.22744	55.44532	-0.64485	0.30754	45.34734
165	0.19815	55.85810	-0.63801	0.27554	46.02070
166	0.34673	56.46843	-0.62780	0.42857	42.88913
167	0.40198	56.97012	-0.61932	0.49438	41.60868
168	0.27920	57.81217	-0.60491	0.36021	44.26065
169	0.09853	58.81596	-0.58743	0.16560	48.41056
170	0.27320	59.96373	-0.56704	0.35089	44.45115
171	0.21954	61.39554	-0.54100	0.29154	45.68272
172	-0.03712	63.28454	-0.50559	0.01747	51.82837
173	-0.02288	67.86279	-0.41472	0.02790	51.57998
174	0.16959	71.99695	-0.32628	0.22561	47.09115
175	0.01764	75.39437	-0.24884	0.06276	50.75841
176	0.16048	78.63686	-0.17076	0.20844	47.46494
177	0.28002	81.10458	-0.10847	0.33064	44.86764
178	0.22287	85.40106	0.00613	0.26593	46.22472
179	0.15854	88.28233	0.08761	0.19610	47.73550
180	0.26191	96.07138	0.32803	0.29494	45.61124
181	-0.06964	103.88288	0.60235	-0.05086	53.48501
182	0.25175	107.50573	0.74246	0.27398	46.05368
183	-0.04978	109.46561	0.82202	-0.03418	53.07573
184	-0.01523	113.14755	0.97918	-0.00130	52.27829
185	0.07742	116.76606	1.14426	0.09044	50.11553
186	0.05217	118.37565	1.22135	0.06401	50.72918
187	-0.03619	120.44662	1.32412	-0.02627	52.88274
188	0.08032	122.55097	1.43290	0.09032	50.11845
189	-0.02916	127.98805	1.73653	-0.02234	52.78715

190	-0.27433	129.25701	1.81257	-0.26926	59.14426	
191	-0.15521	131.58144	1.95750	-0.15026	55.99026	
192	-0.64633	133.88304	2.10880	-0.64359	70.27150	
193	0.23832	125.11958	1.57207	0.24849	46.59750	
194	-0.46787	72.46452	-0.31588	-0.43738	63.90537	
195	-0.44955	64.81431	-0.47603	-0.41353	63.20708	
196	-0.20078	60.90873	-0.54993	-0.15201	56.03531	
197	-0.05695	56.60306	-0.62554	0.00306	52.17343	
198	-0.04438	52.54155	-0.69143	0.02026	51.76172	
199	-0.15768	45.56911	-0.79268	-0.09377	54.55261	
200	-0.52026	43.65326	-0.81795	-0.47379	64.98588	
201	-0.00683	41.22542	-0.84842	0.07096	50.56720	
202	-0.36753	39.36945	-0.87055	-0.31113	60.29583	
203	0.05750	37.09713	-0.89628	0.14410	48.89224	
204	-0.34308	35.76868	-0.91063	-0.28313	59.52332	
205	0.07991	34.97074	-0.91901	0.17035	48.30491	
206	-0.17292	139.33871	2.50297	-0.16998	56.50095	
207	0.52743	137.50490	2.36441	0.53382	40.85990	
208	0.21747	135.57160	2.22515	0.22293	47.14934	
209	0.33177	133.85040	2.10659	0.33853	44.70476	
210	-0.34893	127.35389	1.69930	-0.34367	61.20624	
211	-0.03145	124.77015	1.55271	-0.02338	52.81254	
212	-0.01360	121.95255	1.40150	-0.00417	52.34727	
213	0.11163	118.10464	1.20821	0.12430	49.34022	
214	-0.17127	114.68365	1.04791	-0.15996	56.24100	
215	0.34118	108.41589	0.77907	0.36453	44.17273	
216	0.06747	100.17035	0.46749	0.09166	50.08742	
217	0.09724	81.63482	-0.09476	0.13931	49.00023	
218	0.12455	70.64583	-0.35587	0.17976	48.09608	
219	-0.32173	52.31017	-0.69502	-0.27183	59.21439	
220	-0.01756	39.60106	-0.86784	0.06088	50.80252	
221	0.03072	37.25996	-0.89448	0.11498	49.55230	
222	-0.10339	34.98062	-0.91891	-0.02751	52.91310	
223	0.17434	31.08615	-0.95719	0.27710	45.98762	
224	-0.02616	27.80003	-0.98612	0.06096	50.80062	
225	-0.14058	26.60744	-0.99586	-0.06177	53.75440	
226	0.18079	25.73860	-1.00270	0.28885	45.73951	
227	0.00508	95.00352	0.29322	0.03193	51.48432	
228	-0.05135	86.55782	0.03839	-0.01904	52.70699	
229	-0.71804	82.38889	-0.07505	-0.69874	72.07910	← MAX. OBSERVED
230	0.02324	72.94629	-0.30508	0.07107	50.56467	
231	-0.01943	69.26233	-0.38548	0.03013	51.52704	
232	-0.05336	61.23997	-0.54386	0.00237	52.18984	
233	-0.19570	56.90008	-0.62051	-0.14332	55.81159	
234	-0.06461	52.84772	-0.68664	-0.00149	52.28269	
235	-0.28494	50.52293	-0.72226	-0.23194	58.13638	
236	-0.32116	48.63003	-0.75005	-0.26858	59.12567	
237	-0.18087	43.67140	-0.81772	-0.11685	55.13548	

RADIUS IS 51.79895 MEAN MAG IS 0.01870

APPENDIX IV

CUMULATIVE RESULTS OF ECHO I PHOTOELECTRIC PHOTOMETRY

CUMULATIVE PHOTOELECTRIC RUN ECHO I

INVESTIGATOR: C. L. ROGERS

106 POINTS 2 PASSES, NO. 13 & 17

MEAN MAGNITUDE 0.13504

SIGMA OF THE MAGNITUDES IS 0.17178

CORRELATION COEF. IS 0.15594

STUDENTS T IS 1.60545

MAGNITUDE FOR B # 0 IS, 0.12138

COEF. OF REFLECTIVITY 0.83000 ← ASSUMED FOR RADIUS OF CURVATURE DETERMINATIONS

REGRESSION A IS 3.45301

REGRESSION B IS 0.12385

SPECULAR'ITY [redacted] FROM REGRESSION 0.96538 = 96.5 %

106 PHOTOELECTRIC POINTS

RADIUS	PARAMETRIC SOLUTION INDICATED REFLECTIVITY
40	1.2060202
45	0.9529047
50	0.7718530
55	0.6378951
60	0.5360090

I	MAGNITUDE	ANGLE	MAG. A#0	MSP	RADIUS	
1	0.56752	106.77883	0.87536	0.59622	39.70242	
2	0.45915	106.12054	0.84957	0.48572	41.77501	
3	0.42021	105.56353	0.82798	0.44635	42.53924	
4	0.23078	104.77841	0.79789	0.25332	46.49401	
5	0.22929	101.08136	0.66152	0.25485	46.46134	
6	0.26491	100.38258	0.63669	0.29195	45.67425	
7	0.15249	99.30739	0.59905	0.17771	48.14148	
8	0.06771	98.70277	0.57818	0.09147	50.09184	
9	-0.00695	97.60798	0.54092	0.01600	51.86347	
10	0.21640	96.50100	0.50392	0.24565	46.65853	
11	-0.00141	95.50213	0.47111	0.02320	51.69160	
12	0.17242	94.24252	0.43051	0.20248	47.59530	
13	0.11599	93.48536	0.40650	0.14516	48.86854	
14	0.57174	92.20361	0.36653	0.61815	39.30347	← MINIMUM REDUCED
15	0.20256	91.16689	0.33481	0.23638	46.85821	
16	0.09309	89.73623	0.29191	0.12486	49.32735	
17	0.09182	88.69002	0.26116	0.12448	49.33604	
18	0.16968	88.15499	0.24564	0.20532	47.53306	
19	0.21936	87.36297	0.22291	0.25751	46.40442	
20	0.38512	86.17269	0.18930	0.43112	42.83872	
21	0.18575	85.08503	0.15914	0.22499	47.10452	
22	0.46018	83.88048	0.12637	0.51257	41.26171	
23	0.11002	83.05148	0.10418	0.14850	48.79327	
24	0.11861	82.24846	0.08298	0.15818	48.57624	
25	0.08439	81.56451	0.06513	0.12336	49.36152	
26	0.02279	80.60627	0.04046	0.06044	50.81286	
27	-0.02622	79.64517	0.01610	0.01057	51.99334	
28	0.11348	78.82353	-0.00442	0.15623	48.61995	
29	0.18951	77.02362	-0.04841	0.23737	46.83674	
30	-0.00385	75.77980	-0.07806	0.03718	51.35989	
31	0.38045	75.08591	-0.09434	0.44031	42.65792	
32	0.17025	74.11592	-0.11678	0.22038	47.20472	
33	-0.01869	73.42161	-0.13263	0.02390	51.67497	
34	0.33609	72.17583	-0.16059	0.39720	43.51318	
35	0.15265	71.34961	-0.17882	0.20492	47.54187	
36	0.29760	69.12014	-0.22676	0.36033	44.25823	
37	0.34948	67.88201	-0.25261	0.41702	43.11787	
38	0.06986	62.71226	-0.35473	0.12694	49.28027	
39	0.05045	61.50581	-0.37725	0.10770	49.71889	
40	0.32538	60.18095	-0.40142	0.40143	43.42845	
41	0.31146	59.12021	-0.42035	0.38788	43.70040	
42	0.09615	57.54943	-0.44772	0.16005	48.53441	
43	0.18707	56.38696	-0.46746	0.25806	46.39258	
44	0.07597	55.74428	-0.47819	0.14050	48.97341	
45	0.12299	46.66386	-0.61604	0.19993	47.65119	
46	0.28750	46.32142	-0.62075	0.37798	43.90007	
47	0.35948	45.87343	-0.62686	0.45702	42.33091	
48	0.26409	45.42891	-0.63285	0.35359	44.39588	
49	0.18398	44.65572	-0.64315	0.26769	46.18741	
50	0.40404	44.21322	-0.64896	0.50806	41.34749	
51	0.37562	43.78246	-0.65457	0.47737	41.93597	
52	0.26099	140.22567	2.73413	0.26485	46.24772	
53	0.27919	139.99300	2.71576	0.28318	45.85892	
54	0.17623	139.39926	2.66938	0.18002	48.09019	
55	0.14520	139.12595	2.64827	0.14896	48.78310	
56	0.14020	138.78645	2.62226	0.14403	48.89390	
57	0.16889	137.96279	2.56011	0.17306	48.24470	

58	0.10868	137.50490	2.52613	0.11275	49.60342	
59	0.11577	136.96969	2.48690	0.12001	49.43768	
60	0.12702	136.28132	2.43721	0.13151	49.17666	
61	0.13385	135.78648	2.40202	0.13852	49.01822	
62	0.07511	135.20776	2.36139	0.07970	50.36409	
63	0.09032	134.83816	2.33574	0.09508	50.00849	
64	0.13573	134.00493	2.27876	0.14097	48.96291	
65	0.15664	132.08156	2.15141	0.16265	48.47654	
66	0.16045	131.49140	2.11346	0.16669	48.38629	
67	0.09808	131.01843	2.08342	0.10414	49.80043	
68	0.12281	130.09128	2.02544	0.12935	49.22558	
69	-0.01484	124.66192	1.70845	-0.00712	52.41857	
70	-0.20041	123.67165	1.65444	-0.19358	57.11838	
71	0.00882	121.95255	1.56322	0.01784	51.81938	
72	-0.02988	120.38851	1.48290	-0.02050	52.74259	
73	0.00557	119.13742	1.42039	0.01584	51.86729	
74	-0.04576	117.31189	1.33185	-0.03513	53.09915	
75	-0.18926	115.80816	1.26119	-0.17933	56.74480	
76	-0.04359	113.23249	1.14465	-0.03093	52.99638	
77	-0.13830	112.33837	1.10546	-0.12627	55.37520	
78	0.06724	109.54672	0.98709	0.08348	50.27646	
79	0.07190	107.92372	0.92092	0.08924	50.14320	
80	0.25273	104.34732	0.78155	0.27609	46.00907	
81	0.06159	100.17035	0.62921	0.08412	50.26170	
82	0.17104	95.33604	0.46571	0.20009	47.64770	
83	0.01230	86.83911	0.20804	0.04417	51.19499	
84	0.18946	85.55126	0.17200	0.22837	47.03137	
85	0.29828	77.23366	-0.04335	0.35106	44.44774	
86	0.25697	75.69036	-0.08017	0.30952	45.30605	
87	0.24580	66.32869	-0.28427	0.30887	45.31959	
88	0.52672	62.14171	-0.36544	0.61581	39.34583	
89	0.31482	60.71352	-0.39177	0.38942	43.66934	
90	-0.09539	30.61284	-0.79983	-0.02094	52.75324	
91	-0.12864	27.87940	-0.82375	-0.05485	53.58350	
92	-0.05521	27.19351	-0.82941	0.02436	51.66400	
93	-0.23032	27.00847	-0.83092	-0.16288	56.31659	
94	-0.40086	26.49260	-0.83506	-0.34326	61.19455	← MAXIMUM
95	-0.19293	26.01122	-0.83886	-0.12252	55.27951	REDUCED
96	0.03157	25.94131	-0.83941	0.11887	49.46377	
97	-0.26367	25.79542	-0.84055	-0.19773	VISUAL 57.22779	
98	0.12134	25.75934	-0.84083	0.21663	47.28619	
99	0.07186	25.74763	-0.84092	0.16273	48.47463	
100	0.05762	133.45945	2.24206	0.06266	50.76082	
101	0.11482	132.73879	2.19428	0.12037	49.42947	
102	0.12218	102.56497	0.71522	0.14418	48.89050	
103	0.13207	98.07962	0.55689	0.15780	48.58479	
104	0.10147	93.11991	0.39502	0.13055	49.19828	
105	0.08536	88.96803	0.26928	0.11758	49.49310	
106	-0.13150	28.58083	-0.81781	-0.05833	53.66934	

RADIUS IS 48.21675 FT. MEAN SPECULAR MAG IS 0.17431

NASA-Langley, 1965 CR-200